DISEASES AND DISORDERS

Synoviocyte-targeted therapy synergizes with TNF inhibition in arthritis reversal

Mattias N. D. Svensson[1,2], Martina Zoccheddu[1], Shen Yang[1], Gyrid Nygaard[1], Christian Secchi[1,2,3], Karen M. Doody[2], Kamil Slowikowski[4,5,6,7,8], Fumitaka Mizoguchi[4,9], Frances Humby[10], Rebecca Hands[10], Eugenio Santelli[1,2], Cristiano Sacchetti[1,2], Kuninobu Wakabayashi[11], Dennis J. Wu[1], Christopher Barback[12,13], Rizi Ai[14], Wei Wang[14], Gary P. Sims[15], Piotr Mydel[16,17], Tsuyoshi Kasama[11], David L. Boyle[1], Francesco Galimi[3], David Vera[12,13], Michel L. Tremblay[18,19,20], Soumya Raychaudhuri[4,5,6,7,21,22], Michael B. Brenner[4], Gary S. Firestein[1], Costantino Pitzalis[10], Anna-Karin H. Ekwall[23,24], Stephanie M. Stanford[1,2], Nunzio Bottini[1,2]*

Fibroblast-like synoviocytes (FLS) are joint-lining cells that promote rheumatoid arthritis (RA) pathology. Current disease-modifying antirheumatic agents (DMARDs) operate through systemic immunosuppression. FLS-targeted approaches could potentially be combined with DMARDs to improve control of RA without increasing immunosuppression. Here, we assessed the potential of immunoglobulin-like domains 1 and 2 (Ig1&2), a decoy protein that activates the receptor tyrosine phosphatase sigma (PTPRS) on FLS, for RA therapy. We report that PTPRS expression is enriched in synovial lining RA FLS and that Ig1&2 reduces migration of RA but not osteoarthritis FLS. Administration of an Fc-fusion Ig1&2 attenuated arthritis in mice without affecting innate or adaptive immunity. Furthermore, PTPRS was down-regulated in FLS by tumor necrosis factor (TNF) via a phosphatidylinositol 3-kinase–mediated pathway, and TNF inhibition enhanced PTPRS expression in arthritic joints. Combination of ineffective doses of TNF inhibitor and Fc-Ig1&2 reversed arthritis in mice, providing an example of synergy between FLS-targeted and immunosuppressive DMARD therapies.

INTRODUCTION

Rheumatoid arthritis (RA) is the most common systemic autoimmune disease and is characterized by chronic inflammation, tumor-like enlargement of the joint synovial membrane (called pannus), and progressive destruction of joint cartilage and bone (*1*). Over the past two decades, multiple immunosuppressant disease-modifying antirheumatic drugs (DMARDs) have been approved by the U.S. Food and Drug Administration for the treatment of RA (*2*). Among the most effective are biologic agents blocking the action of the inflammatory cytokine tumor necrosis factor (TNF) (*3*). While immunosuppressive DMARDs are generally very effective, they do increase the risk of infections. In addition, about one-third of patients with RA fail to achieve disease remission, despite trying multiple different immunosuppressants (*4*). Although combining multiple immunosuppressants would likely increase the rates of disease remission, this approach might further increase the risk of infections (*5*, *6*). Thus, there is a current unmet medical need in RA for therapies that can be combined with current DMARDs to spare immunosuppressants or improve control of disease without further suppressing the immune system.

One possible avenue to address this need is to target fibroblast-like synoviocytes (FLS), non-immune cells that reside in the intimal lining of the joint synovium (*7*). FLS are quiescent cells that control the composition of the synovial fluid and the extracellular matrix (ECM) of the joint lining. In RA, however, FLS become invasive, displaying a phenotype characteristic of transformed cells (*7*). RA FLS break down the ECM by producing matrix metalloproteinases, directly invade and digest articular cartilage, promote bone erosion, and enhance inflammation through secretion of interleukin-6 (IL-6), chemokines, and other inflammatory mediators (*7*–*9*). A recent report provided rigorous demonstration that FLS promote arthritis severity in mice and showed that joint lining versus sublining FLS play a different role in experimental arthritis, with lining FLS being critical mediators of cartilage damage and bone erosion (*10*).

It has been suggested that agents selectively targeting RA FLS could be combined with current DMARDs to improve disease control without increasing the risk of infections (*4*, *7*, *11*). However, although a

[1]Department of Medicine, Altman Clinical and Translational Research Institute, University of California, San Diego, La Jolla, CA 92093, USA. [2]Division of Cellular Biology, La Jolla Institute for Immunology, La Jolla, CA 92037, USA. [3]Department of Biomedical Sciences, National Institute of Biostructures and Biosystems, University of Sassari Medical School, 07100 Sassari, Italy. [4]Division of Rheumatology, Immunology, and Allergy, Brigham and Women's Hospital and Harvard Medical School, Boston, MA 02115, USA. [5]Division of Genetics, Brigham and Women's Hospital and Harvard Medical School, Boston, MA 02115, USA. [6]Partners HealthCare Personalized Medicine, Boston, MA 02115, USA. [7]Program in Medical and Population Genetics, Broad Institute of Massachusetts Technical Institute and Harvard University, Cambridge, MA 02138, USA. [8]Bioinformatics and Integrative Genomics, Harvard University, Cambridge, MA 02138, USA. [9]Department of Rheumatology, Graduate School of Medical and Dental Sciences, Tokyo Medical and Dental University (TMDU), Tokyo 113-8519, Japan. [10]Centre for Experimental Medicine and Rheumatology, John Vane Science Centre, William Harvey Research Institute, Barts and The London School of Medicine and Dentistry, Queen Mary University of London, Charterhouse Square, London EC1M 6BQ, UK. [11]Division of Rheumatology, Department of Medicine, Showa University School of Medicine, 1-5-8 Hatanodai, Shinagawa-ku, Tokyo 142-8555, Japan. [12]Department of Radiology, University of California, La Jolla, CA 92093, USA. [13]UCSD Molecular Imaging Program, University of California, La Jolla, CA 92093, USA. [14]Department of Chemistry and Biochemistry, University of California, San Diego, La Jolla, CA 92093, USA. [15]Respiratory, Inflammation and Autoimmunity, Biopharmaceuticals R&D, AstraZeneca, Gaithersburg, MD 20878, USA. [16]Broegelmann Research Laboratory, Department of Clinical Science, University of Bergen, The Laboratory Building, 5th Floor, 5021 Bergen, Norway. [17]Department of Microbiology, Jagiellonian University, Kraków, Poland. [18]Rosalind and Morris Goodman Cancer Research Centre, McGill University, Montréal, Québec H3A 1A3, Canada. [19]Department of Biochemistry, McGill University, Montréal, Québec H3A 1A3, Canada. [20]Department of Medicine, Division of Experimental Medicine, McGill University, Montréal, Québec H3A 1A3, Canada. [21]Rheumatology Unit, Karolinska Institutet, Stockholm S-171 76, Sweden. [22]Institute of Inflammation and Repair, University of Manchester, Manchester M13 9PT, UK. [23]Department of Rheumatology and Inflammation Research, Institute of Medicine, The Sahlgrenska Academy, University of Gothenburg, Gothenburg, Sweden. [24]Centre for Bone and Arthritis Research, Sahlgrenska Academy, University of Gothenburg, Gothenburg, Sweden.
*Corresponding author. Email: nbottini@health.ucsd.edu

few available DMARDs—including Janus kinase (JAK) inhibitors (*12*)—have been shown to reduce FLS aggressiveness, there are currently no therapies available that selectively target FLS. The ideal agent for FLS-directed combination RA therapy would exhibit a mechanism of action independent on innate and adaptive immunity, and its efficacy would not be impaired by concurrent DMARD administration. Thus far, only cadherin-11—an adhesion molecule that acts as a critical regulator of synovial lining formation and FLS signaling—has emerged as a potential target for selective anti-FLS therapy (*13*, *14*).

We recently identified the transmembrane tyrosine phosphatase sigma (PTPRS) as a candidate target for FLS-directed RA therapy (*15*). PTPRS is expressed in the nervous system (*16*, *17*) and stromal cells (*15*, *18*), and its expression in peripheral immune cells from healthy subjects is restricted to plasmacytoid dendritic cells (pDCs) (*19*). PTPRS acts as a receptor for glycosaminoglycan (GAG) moieties of proteoglycans (PGs) in the ECM (*16*, *17*, *20*). Engagement of PTPRS N-terminal extracellular immunoglobulin (IgG)–like domains 1 and 2 (Ig1&2) by ECM PG can modulate PTPRS function through a mechanism that has been termed the PG switch (*16*). PTPRS is highly expressed on FLS, where its function is regulated by an interaction with the heparan sulfate transmembrane PG syndecan-4 (SDC4) (*15*). Disruption of the interaction between PTPRS and syndecan-4 by treatment of FLS with recombinant Ig1&2 decoy protein impaired FLS migration, invasiveness, and attachment to cartilage in a PTPRS-dependent manner (*15*). Furthermore, we demonstrated that treatment with Ig1&2 reversed established arthritis in the K/BxN serum transfer–induced arthritis (STIA) model but was ineffective in PTPRS knockout (KO) mice, providing evidence of target specificity (*15*). These findings suggest potential for PTPRS as a therapeutic target for FLS-directed RA therapy by impairing FLS invasiveness into cartilage.

Here, we assessed the potential of Ig1&2 as an FLS-targeted agent for combination RA therapy. We demonstrate that Ig1&2 has all the features of an ideal agent for FLS-targeted therapy, including target enrichment in lining RA FLS, selective effectiveness on RA FLS versus osteoarthritis (OA) FLS, and efficacy in multiple models of RA without any detectable immunosuppressive mechanism of action. Furthermore, because of the regulatory role of TNF signaling on PTPRS expression in RA FLS, we demonstrate that Ig1&2 can synergize with TNF inhibition in reversing arthritis when administered as a combination therapy.

RESULTS

PTPRS is enriched in lining layer FLS in the RA synovium

To further establish PTPRS as a target for FLS-directed therapy for RA, we first examined the expression profile of PTPRS in the rheumatic synovium. As shown in Fig. 1A, immunofluorescent (IF) staining revealed prominent expression of PTPRS in the lining layer of the RA synovium and only sparse staining in the sublining, which was confirmed by immunohistochemical staining for PTPRS (fig. S1, A and B). Furthermore, staining for PTPRS was mainly found to colocalize with podoplanin staining on cells within the lining layer of the synovium (Fig. 1A and fig. S1A). As podoplanin is considered to be a marker for aggressive FLS in RA (*21*), these results suggest that PTPRS expression is mainly found on aggressive FLS within the lining layer of the RA synovium. Consistent with our previous report that PTPRS expression is induced by chronic inflammatory arthritis in mice (*15*), no expression of PTPRS was observed in the synovial tissue from patients with OA, which correlated with a lack of podoplanin expression (Fig. 1A). The enriched expression of *PTPRS* in synovial lining RA FLS [$CDH11^+CD34^-THY1^-$ (*22*)] when compared to sublining RA FLS [$CDH11^+CD34^-THY1^+$ (*22*)] was further confirmed by mining RNA sequencing (RNA-seq) data from RA FLS freshly isolated from the synovial tissue of patients with RA (Fig. 1B) (*22*).

Ig1&2 inhibits motility of RA FLS but not OA FLS

To increase the therapeutic potential and drug-like properties of Ig1&2, we generated an Fc-fused Ig1&2 by replacing our previously described 6xHis-tag (*15*) at the protein C terminus with a human IgG1 Fc (Fig. 1C). Fc-Ig1&2 showed similar efficacy in suppressing RA FLS migration in vitro as His-Ig1&2, an effect that was not mediated through the Fc portion of the protein (fig. S1C). In addition, Fc-Ig1&2 was effective in limiting invasion of RA FLS through type I collagen–based matrix (Fig. 1D). This effect on Fc-Ig1&2 of FLS migration and invasion was not due to an alteration in cell numbers, because Fc-Ig1&2 did not affect RA FLS proliferation (fig. S1D).

To assess whether the mechanism of action of Ig1&2 is selective for RA FLS, we next compared the effect of Ig1&2 on the migratory potential of RA FLS versus OA FLS and normal human dermal fibroblasts (NHDF) using a scratch wound assay. Although Fc-Ig1&2 was very effective in inhibiting the migration and invasion of RA FLS in response to serum, unexpectedly, it did not alter the migratory and/or invasive potential of OA FLS or/and NHDF (Fig. 1, E to G, and fig. S1, E to H). Although a notable difference in expression of PTPRS was observed between RA and OA synovium (Fig. 1A), RA and OA FLS unexpectedly displayed similar mRNA expression of *PTPRS* [(*15*) and fig. S1I]. The higher expression of PTPRS in cultured versus synovial OA FLS is likely due to cell confluency, which we have previously shown an important inducer of PTPRS expression (*15*). However, we cannot, at the moment, rule out positive selection of high PTPRS expressor OA FLS subsets during culturing and/or modulation of PTPRS expression by the local OA microenvironment. Nevertheless, our results point to cultured RA FLS having a distinct phenotype from OA FLS, which renders them susceptible to PTPRS-mediated migratory inhibition.

We have previously shown that the effect of Ig1&2 is critically dependent on the PG syndecan-4 (*15*). Consistent with the selective effect of Ig1&2 on RA FLS, we found an increased expression of *SDC4* in RA FLS when compared to both OA FLS and NHDF (fig. S1, J and K). We next explored the epigenomic and transcriptomic landscape of the *SDC4* locus in RA and OA FLS using our recently published dataset (*23*). We found that RA FLS showed a 1.2-fold increased signal ($P < 0.01$) for the epigenetic histone mark H3K4me3 (Fig. 1, H and I), which associates with transcriptional start sites of actively transcribed genes (*24*). Such increased signal was associated with increased RNA-seq expression signal (1.4-fold, $P < 0.05$) for *SDC4* in RA FLS from the same dataset (Fig. 1J). Together, these results suggest that the effect of Ig1&2 is specific to RA FLS because of an epigenetically driven increased expression of syndecan-4.

Fc-Ig1&2 shows high accumulation in arthritic paws and suppresses experimental arthritis

Next, we sought to characterize the efficacy of Fc-Ig1&2 in experimental mouse arthritis. Similar to results for 6xHis-Ig1&2 (*15*), we found that Fc-Ig1&2 was highly effective in suppressing K/BxN STIA development in mice (fig. S2A). To gain a deeper insight into the

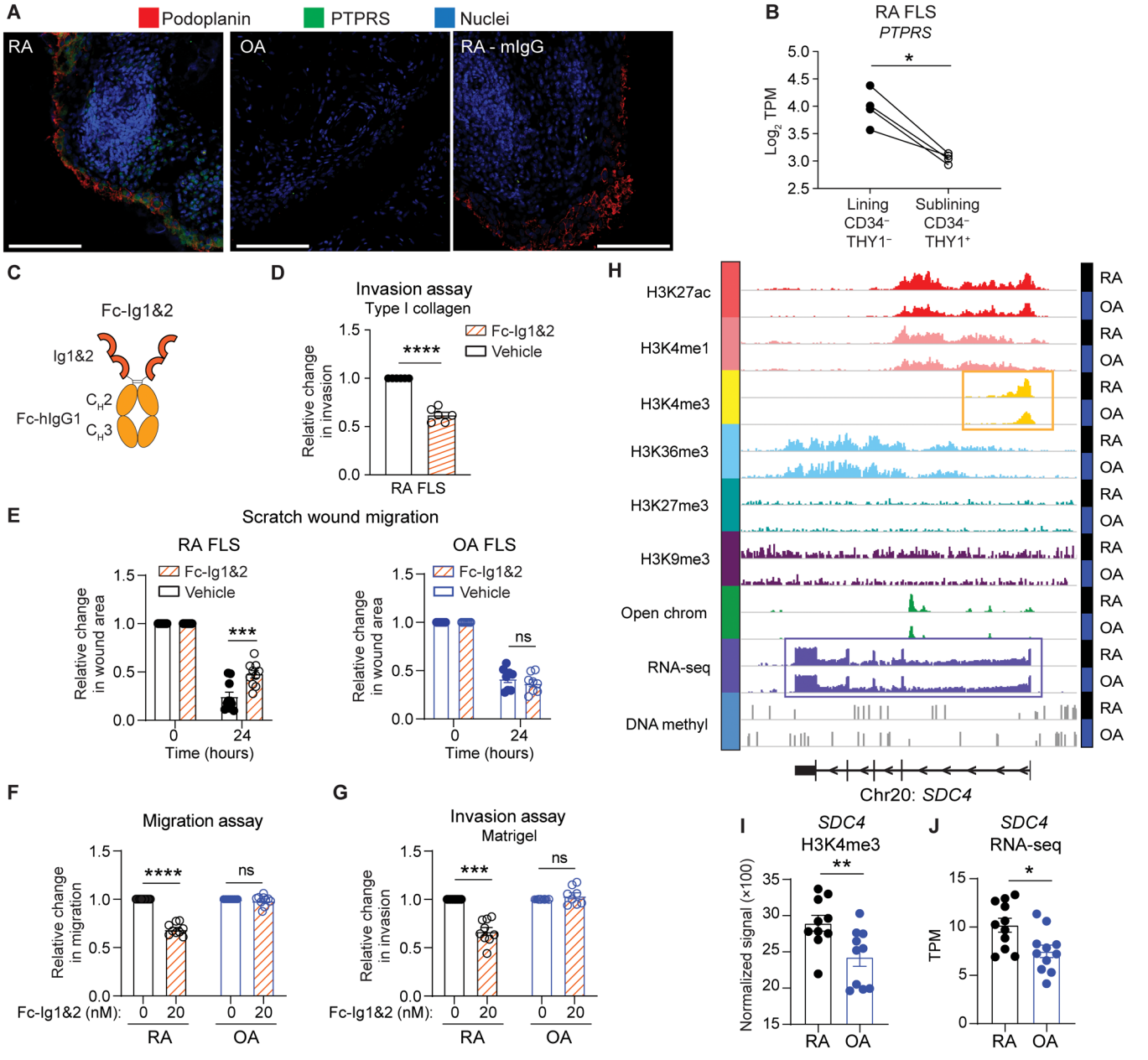

Fig. 1. Ig1&2 selectively inhibits the aggressive behavior of RA FLS but not OA FLS. (**A**) Representative IF images of expression of PTPRS (green) and podoplanin (red) expression in RA ($n = 5$) and OA ($n = 4$) synovial tissue. Hoechst was used for nuclear stain and mouse IgG (mIgG) as control for PTPRS. Scale bar, 100 μm. (**B**) Expression of *PTPRS* by RNA-seq in lining (cadherin-11$^+$CD34$^-$THY$^-$) and sublining (cadherin-11$^+$CD34$^-$THY$^+$) layer FLS isolated from RA synovial tissue ($n = 7$). TPM, transcripts per million. (**C**) Scheme of human Fc-Ig1&2 fusion protein. (**D**) Invasion of RA FLS ($n = 6$) through type I collagen in response to 10% FBS in the presence or absence of Fc-Ig1&2 (20 nM). (**E**) Wound healing by RA ($n = 10$) and OA ($n = 8$) FLS in response to 1% FBS in the presence or absence of Fc-Ig1&2 (20 nM). ns, not significant. (**F** and **G**) Transwell migration (F) and invasion through Matrigel (G) by RA (migration, $n = 9$; invasion, $n = 9$) and OA (migration, $n = 10$; invasion, $n = 8$) FLS in response to 10% FBS in the presence or absence of Fc-Ig1&2. (**H**) Epigenomic landscape of the syndecan-4 (*SDC4*) locus in representative OA and RA FLS lines. (**I** and **J**) H3K4me3 signal in *SDC4* (I) and *SDC4* expression by RNA-seq (J) in RA ($n = 10$) and OA ($n = 10$) FLS. (D to G) Fold change relative to vehicle-treated controls. Graphs represent means ± SEM. *$P < 0.05$, **$P < 0.01$, ***$P < 0.001$, and ****$P < 0.0001$ by Mann-Whitney (B, I, and J) or paired ratio *t* test (D to G) calculated on non-normalized data.

biodistribution of Fc-Ig1&2 during arthritis, we injected 111-indium (^{111}In)–labeled Fc-Ig1&2 in mice with established STIA. Radiolabeling of Fc-Ig1&2 did not affect the function of the protein (fig. S2B). As controls, we used an ^{111}In-labeled murine homolog of etanercept (murine p75TNFR:Fc; here called Fc-mTNFR) (Fig. 2A and fig. S2B). As shown in Fig. 2, A and B, Fc-Ig1&2 showed significantly increased accumulation in the joints of arthritic mice in comparison to Fc-mTNFR. ^{111}In-Fc-Ig1&2 was nearly absent in mouse brains and eyes, suggesting that Fc-Ig1&2 does not cross the blood-brain barrier (fig. S2C).

We next assessed the efficacy of Ig1&2 in reversal of mouse collagen-induced arthritis (CIA), which is driven by the adaptive immune system and considered the gold standard for preclinical therapeutic development for RA (*25*). Administration of Fc-Ig1&2 to arthritic CIA mice caused a significant reduction in disease severity, comparable

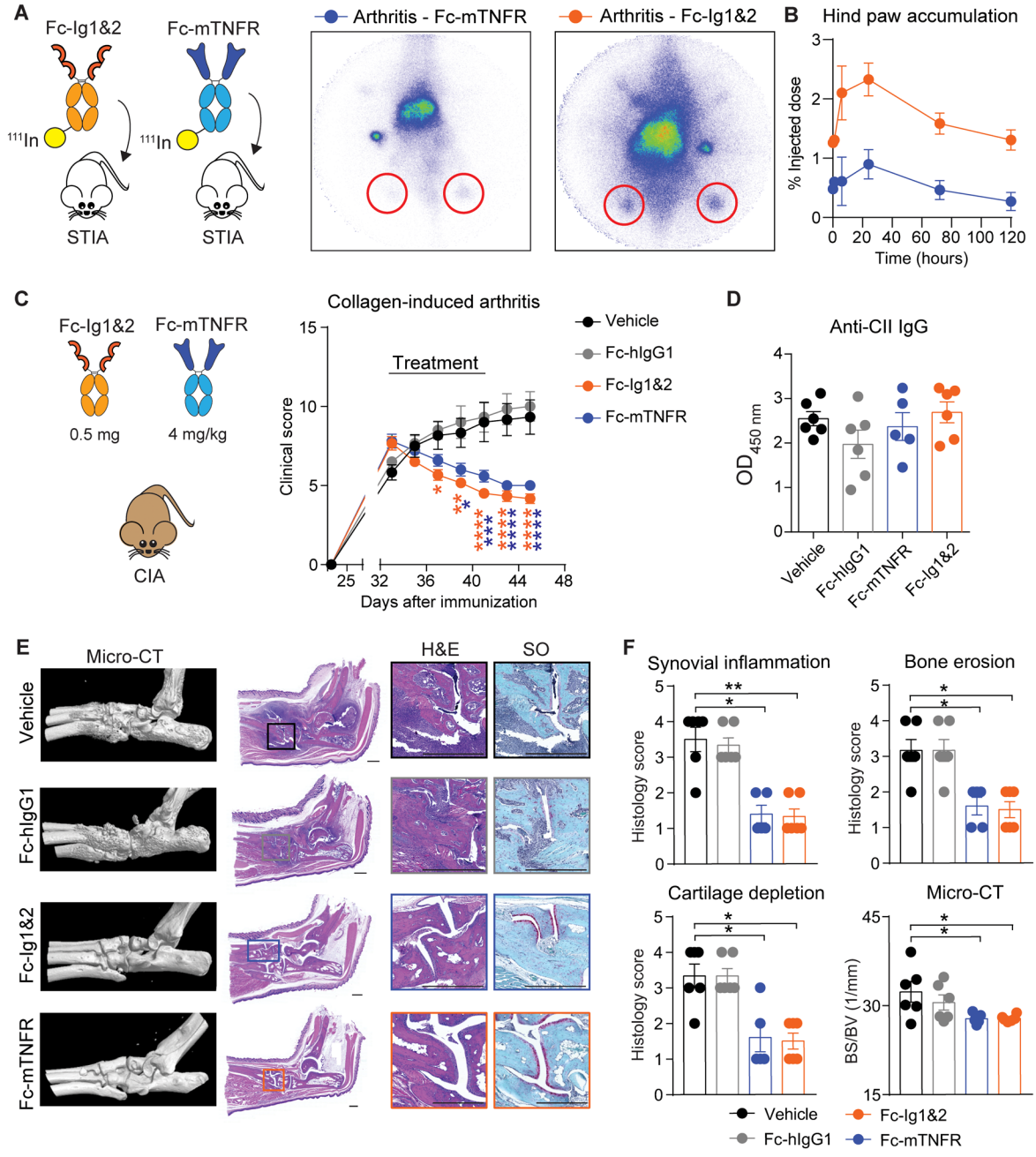

Fig. 2. Fc-Ig1&2 accumulates in arthritic ankles and suppresses development of arthritis. (**A**) BALB/c mice with established STIA were intravenously injected with the same amount of either ^{111}In-labeled Fc-mTNFR (280 μCi; $n = 5$) or Fc-Ig1&2 (165 μCi; $n = 4$). Representative images of measurement 6 hours after injection. (**B**) Comparison of accumulation of labeled proteins from (A) in hind paws of arthritic mice. (**C**) Clinical score of DBA/1J mice with CIA treated with either 0.5 mg of Fc-Ig1&2 ($n = 6$), Fc-mTNFR (4 mg/kg; $n = 6$), 0.5 mg of human IgG1-Fc control (Fc-hIgG1; $n = 6$), or vehicle ($n = 6$) by intraperitoneal injection once every other day for a total of five treatments as indicated. (**D**) Serum level of anti-collagen antibodies of mice in (C). OD, optical density. CII, type II collagen. (**E** and **F**) Representative Micro-CT, hematoxylin and eosin (H&E), and Safranin O (SO) images used for quantification (F) of synovial inflammation, bone erosion, and cartilage depletion of mice in (C). Scale bars, 500 μm. Bone erosions were evaluated by Micro-CT by measuring the change in bone surface (BS) divided by bone volume (BV) (1/mm). Graphs represent means ± SEM. *$P < 0.05$, **$P < 0.01$, ***$P < 0.001$, and ****$P < 0.0001$ by two-way analysis of variance (ANOVA) [(C) orange asterisks indicate significance for Fc-Ig1&2 versus Fc-IgG1 and vehicle, while blue stars indicate significance for Fc-mTNFR versus Fc-IgG1 and vehicle] or Kruskal-Wallis (D).

to treatment with Fc-mTNFR using a dose (4 mg/kg) that has been shown to be effective in CIA (Fig. 2C) (*26*). The efficacy of Fc-Ig1&2 in CIA was not associated with decreased production of anti-collagen antibodies (Fig. 2D). Fc-Ig1&2 administration also protected mice from inflammation (2.6-fold reduction, $P < 0.01$), cartilage damage (2.2-fold reduction, $P < 0.05$), and bone erosions (2.1-fold reduction, $P < 0.05$) as assessed by histopathology and micro–computed tomography (Micro-CT) analysis of joints (1.2-fold reduction, $P < 0.05$; Fig. 2, E and F). Together, these results suggest that Ig1&2 has a favorable biodistribution profile and exerts a therapeutic effect

in multiple models of arthritis driven by the innate and/or adaptive immune system.

Ig1&2 attenuates inflammatory arthritis without suppressing the innate immune system

We next sought to thoroughly characterize whether the therapeutic effect of Ig1&2 is mediated through suppression of the innate or adaptive immune system. Previous transcriptomic studies have suggested that PTPRS expression is virtually absent from the majority of immune cells in healthy humans and mice, with the exception of pDCs (*19*).

To evaluate whether the effect of Ig1&2 is mediated through the innate immune system, we used again the STIA model, in which disease pathogenesis is heavily dependent on the actions of FLS and innate immune cells but independent of adaptive immune cells (*13*, *27*). Nonclassical Ly6C$^-$ monocytes and bone marrow–derived major histocompatibility complex II$^+$ (MHCII$^+$)CD64$^+$ macrophages are crucial mediators of arthritis in this model, while tissue-resident MHCII$^-$CD64$^+$ macrophages play a protective role (*28*). However, neither classical (Ly6C$^+$CD43$^-$), intermediate (Ly6C$^+$CD43$^+$), or nonclassical (Ly6C$^-$CD43$^+$) circulating monocytes showed detectable expression of PTPRS (fig. S3A) in STIA mice. Furthermore, PTPRS was absent on MHCII$^+$CD64$^+$ macrophages and expressed at low levels in a small subset of MHCII$^-$CD64$^+$ macrophages isolated from arthritic ankles of STIA mice (fig. S3A). Next, to dissect the effect of Ig1&2 on FLS versus radiosensitive bone marrow–derived cells in vivo, we compared the efficacy of Ig1&2 at attenuating STIA in CD45.1 congenic mice subjected to lethal irradiation [>10 gray (Gy)] and bone marrow transplantation from CD45.2 wild-type (WT) or PTPRS KO mice (Fig. 3A and fig. S3B). Mice reconstituted with WT or KO bone marrow displayed identical arthritis severity once subjected to STIA (Fig. 3A). Furthermore, Ig1&2 displayed identical anti-arthritic action in the two groups of mice (Fig. 3A). To complete our assessment of whether innate immunity mediates the anti-arthritic action of Ig1&2, we turned to pDC, which express high levels of PTPRS [(*19*) and fig. S3A]. To assess whether pDC contribute to the anti-arthritic action of Ig1&2 in vivo, we depleted pDC using an anti–PDCA-1 (plasmacytoid dendritic cell antigen-1) antibody (*29*) before subjecting mice to STIA (fig. S3C). We found no difference in arthritis development between pDC-depleted and nondepleted mice, and the anti-arthritic effect of Ig1&2 was maintained in pDC-depleted mice (fig. S3D).

To further rule out any potential effects of Ig1&2 on activated macrophages, we also evaluated macrophage polarization and bacterial phagocytosis. First, Fc-Ig1&2 was added during the polarization of bone marrow–derived macrophages (BMDMs) into either M1 or M2 effector phenotypes. For both effector phenotypes, the addition of Fc-Ig1&2 did not affect the up-regulation of characteristic transcription factors or cytokines (fig. S4, A and B). Similarly, Fc-Ig1&2 did not alter the phagocytosis of either *Escherichia coli* or *Staphylococcus aureus* by M0, M1, or M2 macrophages (fig. S4, C and D). This suggests that Ig1&2 does not alter functions of innate immune cells and that its therapeutic effect in mouse arthritis is not mediated through suppression of the innate immune system.

The therapeutic effect of Ig1&2 in mouse arthritis is not mediated through the adaptive immune system

We next assessed whether Ig1&2 exerts an effect on arthritis development through an action on the adaptive immune system. First,

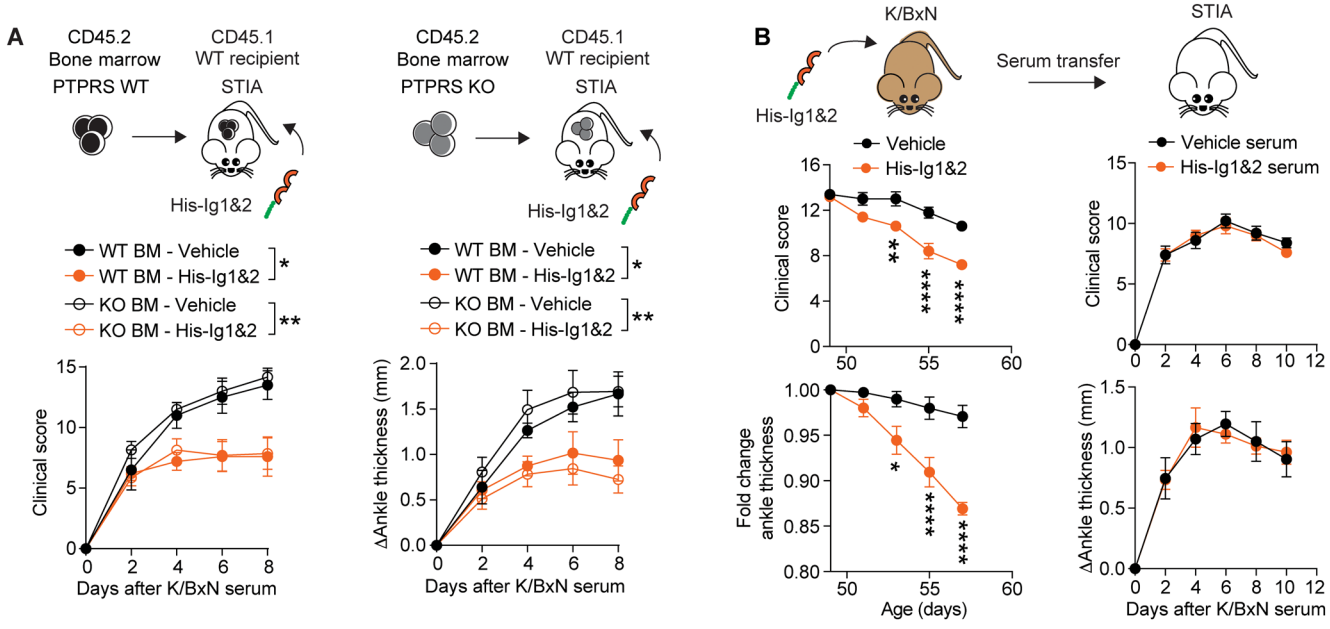

Fig. 3. The therapeutic effect of Ig1&2 in K/BxN arthritis is not mediated through the immune system. (**A**) Top panel shows scheme for evaluating the effect of Ig1&2 on development of K/BxN STIA in WT mice reconstituted with either PTPRS WT or KO bone marrow (BM). Mice were treated with either vehicle or 0.5 mg of histidine tagged Ig1&2 (His-Ig1&2) by retro-orbital (r.o.) injection once every other day for a total of four treatments. Clinical score (left bottom panel) and change in ankle swelling (right bottom panel) is shown for groups; WT BM treated with vehicle ($n = 4$), WT BM treated with His-Ig1&2 ($n = 5$), KO BM treated with vehicle ($n = 6$), and KO BM treated with His-Ig1&2 ($n = 7$). (**B**) At 7 weeks of age, mice with active K/BxN arthritis were treated with 0.5 mg of His-Ig1&2 ($n = 5$) or vehicle ($n = 5$) r.o. every 2 days for a total of four treatments. After 10 days, sera were collected, and 100 μl was used to induce STIA in BALB/c mice ($n = 5$ per group). Arthritis in K/BxN and BALB/c mice was assessed by clinical scoring (top) and change in ankle thickness (bottom). Arthritis severity in (A) calculated using area under the curve. *$P < 0.05$, **$P < 0.01$, ***$P < 0.001$, and ****$P < 0.0001$ by Mann-Whitney (A) or two-way ANOVA (B).

we administered Ig1&2 to arthritic K/BxN transgenic mice, which develop spontaneous arthritis starting at 6 to 7 weeks of age (*27*). We observed a significant reversal of spontaneous arthritis in these mice after treatment with Ig1&2 (Fig. 3B). However, when sera of Ig1&2-treated K/BxN mice were transferred into WT recipient mice to induce STIA, we did not observe any difference in the arthritogenicity of sera from the Ig1&2-treated versus vehicle-treated K/BxN mice (Fig. 3B). Thus, reversal of spontaneous K/BxN arthritis by Ig1&2 is not mediated by decreased titers of arthritogenic antibodies.

Next, we used mouse CIA to further determine the effect of Fc-Ig1&2 on the adaptive immune system during arthritis. The therapeutic efficacy of Fc-Ig1&2 was not associated with an altered accumulation or expansion of regulatory T cells (T_{regs}) or T helper 17 (T_H17) cells in arthritic ankles of CIA mice (Fig. 4, A and B, and fig. S5A). Consistent with the STIA data, treatment with therapeutic doses of Fc-Ig1&2 did not alter the number or frequency of $MHCII^+CD64^+$ and $MHCII^-CD64^+$ macrophages in the same ankles (Fig. 4C and fig. S5B). Furthermore, the therapeutic effect of Fc-Ig1&2 was not associated

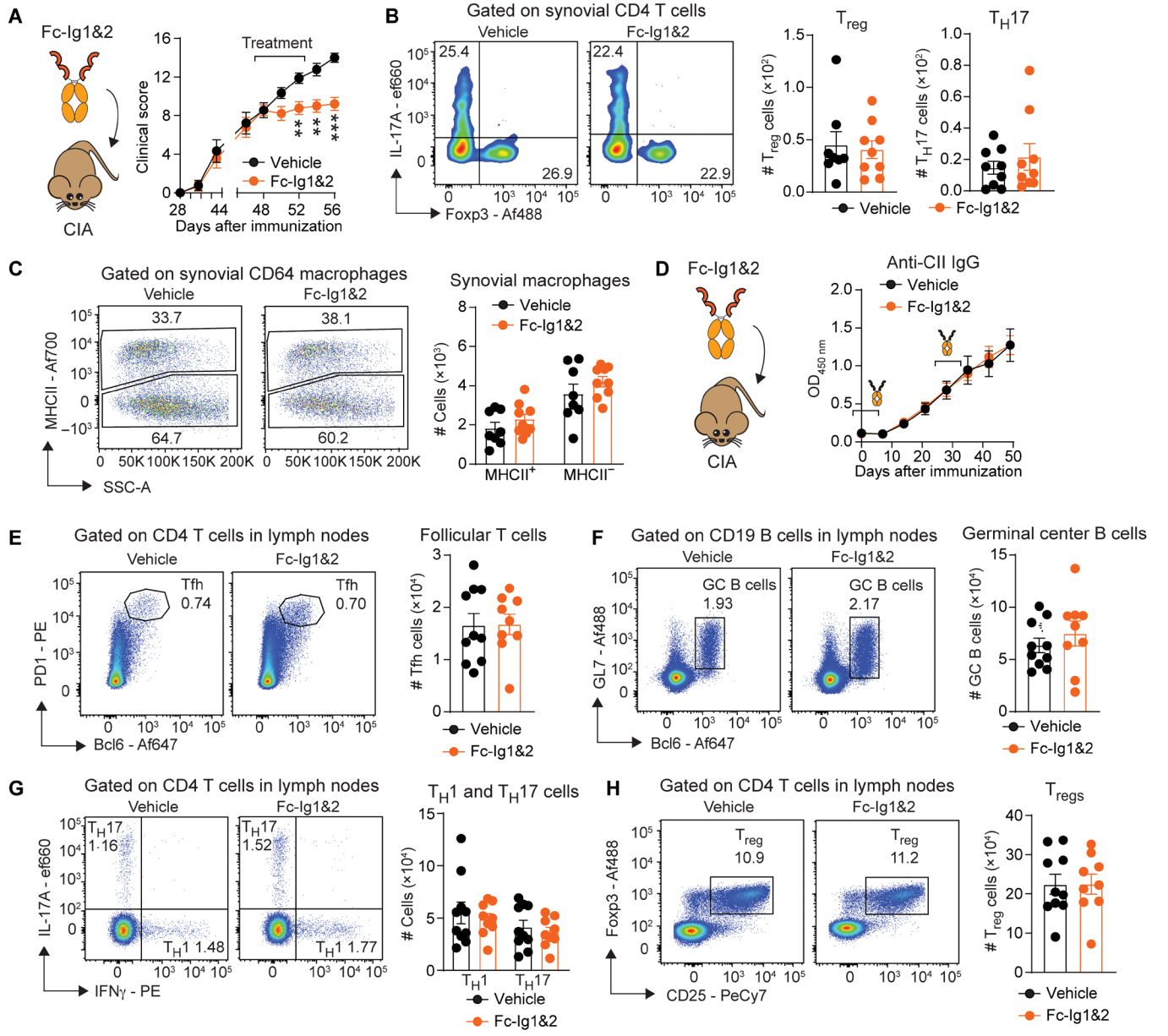

Fig. 4. The therapeutic effect of Ig1&2 in CIA is not mediated through the immune system. (**A**) Therapeutic treatment of DBA/1J mice with CIA by intraperitoneal injections of 0.5 mg of Fc-Ig1&2 ($n = 9$) or vehicle control ($n = 8$) every other day for a total of three injections. Mice were euthanized 4 days after the last treatment, which corresponds to 56 days after primary immunization. (**B**) Number of regulatory T cells (T_{regs}; $Tcr\beta^+CD4^+IL\text{-}17^-FoxP3^+$) and T_H17 ($Tcr\beta^+CD4^+IL\text{-}17^+FoxP3^-$) cells in arthritic ankles isolated from mice in (A). (**C**) $MHCII^+$ and $MHCII^-$ (tissue-resident) synovial macrophages ($CD45^+CD11b^+Ly6G^-Ly6C^-CD64^+$) in arthritic ankles isolated from mice in (A). (**D**) Treatment of DBA/1J mice by intraperitoneal injections with either 0.5 mg of Fc-Ig1&2 ($n = 9$) or vehicle control ($n = 10$) during the primary and boost collagen immunization. Mice were treated every other day with one treatment the day before immunization and two treatments after immunization. (**E** to **H**) Number of follicular T cells [(Tfh); (E)], GC B cells (F), T_H1 and T_H17 cells (G), and T_{regs} (H) in joint draining lymph nodes of mice in (D). Graphs represent means ± SEM. $^{**}P < 0.01$ and $^{***}P < 0.001$ by two-way ANOVA (A). PD-1, programmed cell death; PE, phycoerythrin.

with an alteration in the expansion of naïve and effector CD4 T cells or the expansion of the CD4 T cell effector populations T_H1 or T_H17 cells in the spleen and lymph nodes of arthritic CIA mice (fig. S5, C to F). Similarly, we did not observe any effects on germinal center (GC) B cell or CD4 T follicular helper (Tfh) cell numbers (fig. S5, G to J), which are important for the generation of pathogenic autoantibodies in the CIA model (*30*). Last, there was no change in T_{reg} numbers or in the expression of CTLA4 by T_{regs}, in arthritic CIA mice after treatment with Fc-Ig1&2 (fig. S5, K and L). Together, these results suggest that the therapeutic action of Fc-Ig1&2 in CIA is not mediated through an effect on CD4 effector populations or GC B cells.

Ig1&2 does not alter adaptive responses to immunization

To determine whether Ig1&2 could potentially affect the immune response following immunization—which is affected by immunosuppressive DMARDs (*31*)—we next treated DBA/1J mice with Fc-Ig1&2 during the primary and boost immunization against type II collagen and followed the generation of anti-collagen type II antibodies (fig. S6A). Consistent with the data shown in Fig. 2D, we did not observe any effect of Fc-Ig1&2 on overall titers of anti-collagen IgG antibodies (Fig. 4D) or the titers of anti-collagen IgG subclasses IgG1, IgG2a, IgG2b, and IgG3 (fig. S6B). We also did not observe any effect of Fc-Ig1&2 on the frequency and numbers of Tfh cells or GC B cells (Fig. 4, E and F, and fig. S6, C and D). Together, these results suggest that Ig1&2 does not affect humoral responses to immunization with type II collagen.

Ig1&2 does not alter the polarization of CD4 T cells

Recently, it was shown that PTPRS KO CD4 T cells show enhanced polarization into T_H1 and T_H17 cells (*32*). To determine whether Ig1&2 affects CD4 T cell polarization during immunization with collagen, we evaluated CD4 T cell populations in mice treated with Fc-Ig1&2 during primary and boost immunizations. We did not observe skewing of naïve or effector CD4 T cell populations in the spleen and lymph nodes of Fc-Ig1&2–treated mice (fig. S6, E and F). Also, we did not observe any alterations in the numbers of T_H1, T_H17, or T_{regs} in either lymph nodes (Fig. 4, G and H, and fig. S6H) or spleen (fig. S6, G and H) of the same mice. T_{regs} from lymph nodes and spleen of mice treated with either Fc-Ig1&2 or vehicle displayed similar levels of CTLA4 (cytotoxic T-lymphocyte-associated protein 4) expression (fig. S6H). To further dissect the effect of Ig1&2 on the polarization of CD4 T cells, we performed in vitro polarization assays of CD4 T cells stimulated with plate-bound antibodies or antigen-presenting cells (APCs). Similar to our in vivo observations, Ig1&2 did not alter the polarization of CD4 T cells isolated from BALB/c or DBA/1J mice into T_H1, T_H17, or T_{reg} cells, regardless of the presence or absence of APCs (fig. S7, A to D). Together, these results suggest that Ig1&2 does not affect the polarization of CD4 T cells in vitro or in vivo and support the idea that the therapeutic effect of Fc-Ig1&2 is unlikely to be mediated through immunosuppression.

TNF down-regulates PTPRS expression in RA FLS and decreases their sensitivity to Ig1&2

TNF inhibitors are a major class of immunosuppressive DMARDs for treatment of RA. To evaluate whether Ig1&2 could be used in combination with anti-TNF therapy, we first determined whether TNF modulates PTPRS expression. As shown in Fig. 5 (A to C), stimulation with TNF caused concentration and time-dependent down-regulation of PTPRS expression in RA FLS at the mRNA and protein level, which was unaffected by the presence of normal growth media during TNF stimulation (fig. S8A). This effect of TNF on the expression of *PTPRS* at the mRNA level was further confirmed a Japanese cohort of RA FLS and in mouse FLS (fig. S8, B and C). In addition, activation of RA FLS with knee synovial fluids from patients with active RA—as shown by the increased production of *IL6*—resulted in a reduction of *PTPRS* (Fig. 5D and fig. S8D). Consistent with the inhibitory effect of TNF on PTPRS expression in RA FLS, we found a negative correlation between the mRNA expression of *PTPRS* and *TNF* quantified by quantitative polymerase chain reaction (qPCR) in the synovial tissue of patients with RA (Fig. 5E and fig. S8E). Down-regulation of PTPRS expression by TNF correlated with reduced sensitivity of RA FLS to migration inhibition by Ig1&2. However, consistent with the efficacy of Ig1&2 in the TNF-enriched joints of CIA mice, TNF-treated RA FLS retained significant responsiveness to ≥10 nM Ig1&2 in motility assays in vitro (Fig. 5, F to H). We conclude that, although TNF stimulation might reduce the sensitivity of RA FLS to Ig1&2, sufficient expression of PTPRS is retained on TNF-stimulated RA FLS to limit their motility once the cells are incubated with optimal amounts of PTPRS-activating Ig1&2.

TNF regulates PTPRS expression in RA FLS through the PI3K/GSK3β/USF2 pathway

The regulation of *PTPRS* expression has not yet been addressed. To further investigate the potential signaling pathway by which TNF affects *PTPRS* expression, we inhibited two TNF-dependent pathways—the nuclear factor κB (NFκB) and phosphatidylinositol 3-kinase (PI3K) signaling pathways—in RA FLS. Inhibition of the NFκB pathway had no effect on the expression of *PTPRS* after TNF stimulation (Fig. 6A). However, inhibition of PI3K prevented down-regulation of *PTPRS* induced by TNF. Previous studies have identified that PI3K is required for TNF-induced activation of AKT in RA FLS and important for the proliferation, migration, and invasion of RA FLS (*33*). Inhibition of glycogen synthase kinase 3β (GSK3β) through phosphorylation at Ser^9 is a major consequence of PI3K/AKT pathway activation (*34*), and increased GSK3β $pSer^9$ phosphorylation correlates with increased activation of the PTPRS-target ezrin in RA FLS (*33*, *35*). Accordingly, inhibition of GSK3β resulted in significant down-regulation of *PTPRS* expression in resting RA FLS (Fig. 6B). Further evaluation of the epigenomic landscape of the *PTPRS* locus in RA FLS [n = 10; data from our recently published dataset, (*23*)] revealed histone marks for active promoters (H3K4me3), primed enhancers (H3Kme1), and repressive marks (H3K27me3) around exon 1 of the *PTPRS* gene. Using the ENCODE (Encyclopedia of DNA Elements) database and the University of California, Santa Cruz (UCSC) human genome browser, we identified potential binding sites for two downstream targets of GSK3β, upstream stimulatory factor 1 (USF1) and USF2 (*36*), in the promoter region of *PTPRS*, suggesting involvement of these two transcription factors in the regulation of PTPRS expression (Fig. 6C). This was further supported by a positive correlation between the expression of either *USF1* or *USF2* with *PTPRS* in RA and OA FLS, as detected by analysis of our recently published RNA-seq data (fig. S9A) (*23*). By using small interfering RNA (siRNA)–mediated knockdown of *USF2*, we found that USF2 indeed promotes the expression of *PTPRS* in RA FLS (Fig. 6D and fig. S9B). Using chromatin immunoprecipitation (ChIP), we further confirmed that USF2 binds the promoter region of *PTPRS* in resting RA FLS

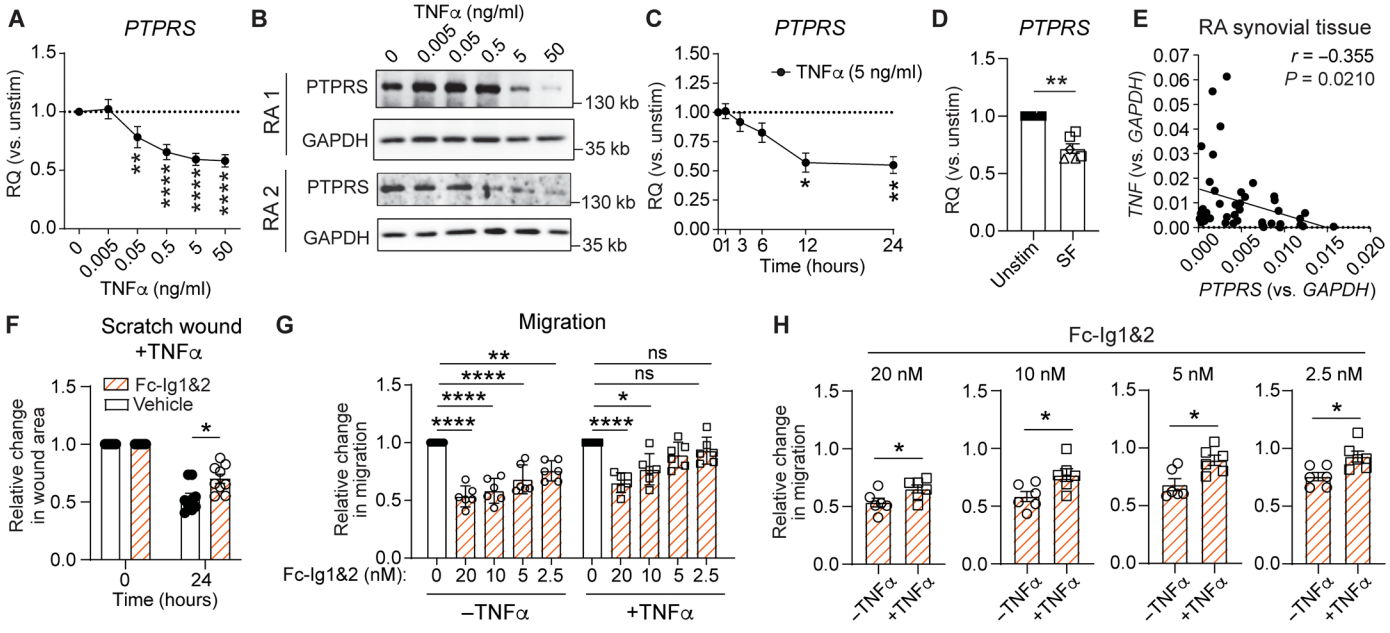

Fig. 5. TNF down-regulates expression of PTPRS in RA FLS. (**A** and **B**) Gene (A) and protein (B) expression of *PTPRS* in RA FLS ($n = 13$) stimulated with TNFα for 12 [gene, (A)] or 24 hours [protein, (B)]. RQ, relative quantification. (**C**) Time-dependent down-regulation of *PTPRS* in RA FLS ($n = 7$) stimulated with TNFα (5 ng/ml). (**D**) Expression of *PTPRS* in RA FLS ($n = 6$) stimulated with synovial fluid (SF) obtained from three individual patients with RA with active disease RA1 (squares; $n = 3$ FLS lines), RA2 (triangles; $n = 2$ FLS lines), and RA3 (diamond; $n = 1$ FLS line) for 12 hours. (**E**) Correlation between expression of *TNF* and *PTPRS* in RA synovial tissue ($n = 42$). Linear regression is shown. (**F**) RA FLS were stimulated with TNFα (50 ng/ml) for 24 hours, after which scratch-wounding healing was evaluated in response to 1% FBS and TNFα (50 ng/ml) in the presence or absence of 20 nM Fc-Ig1&2. (**G**) RA FLS were prestimulated with TNFα (50 ng/ml) for 24 hours, after which cells were subjected to transwell migration in response to 10% FBS in the presence or absence of TNFα (50 ng/ml) and Fc-Ig1&2. (**H**) Relative change in migration between RA FLS migrated in the presence or absence of TNFα and Fc-Ig1&2. Gene expression in (A), (C), (D), and (E) relative to *GAPDH*. Graphs represent means ± SEM. $^*P < 0.05$, $^{**}P < 0.01$, and $^{****}P < 0.0001$ by paired one-way ANOVA (A, C, and G), Mann-Whitney (H), Spearman correlation (E), or paired ratio *t* test (D) calculated on non-normalized data.

and that such interaction was significantly reduced after stimulation with TNF (Fig. 6E and fig. S9C). Last, using a luciferase reporter construct encompassing the *PTPRS* promoter region, we demonstrated that overexpression of USF2 causes a strong activation of the PTPRS promoter (Fig. 6F). Together, these results suggest that expression of PTPRS in RA FLS is regulated by TNF via a PI3K/GSK3β/USF2 pathway.

Therapeutic synergy between Fc-Ig1&2 and Fc-mTNFR in CIA

The inverse correlation between TNF stimulation and PTPRS expression in RA FLS suggests the intriguing scenario where combination therapy with TNF inhibitors could synergize with Ig1&2 by inducing PTPRS expression on RA FLS. To test this hypothesis experimentally, we first determined whether TNF inhibition induces the expression of PTPRS in CIA joints. An initial dose response of Fc-mTNFR in CIA showed that a clinically ineffective dose of Fc-mTNFR (2 mg/kg) was sufficient to enhance *Ptprs* expression in arthritic joints of mice (fig. S10, A and B).

Next, to evaluate the potential synergy between Ig1&2 and TNF inhibition in CIA, we treated arthritic CIA mice with either a suboptimal dose of Fc-Ig1&2 (0.1 mg), Fc-mTNFR (2 mg/kg), or a combination of the two (Fig. 7A). Monotherapy with either suboptimal Fc-Ig1&2 or Fc-mTNFR (2 mg/kg) did not cause significant reversal of disease in CIA. However, the combination of the two clinically ineffective doses of Fc-Ig1&2 and Fc-mTNFR caused a notable reversal of clinical CIA (Fig. 7A). The combination therapy, but not the monotherapies, also protected mice from cartilage damage and bone erosions, as assessed by histopathologic analysis of joints (Fig. 7, B and C). Consistent with the lack of effect of Fc-Ig1&2 on the abovementioned adaptive immune responses, the combined Fc-mTNFR–Fc-Ig1&2 treatment did not lead to a reduction in anti-collagen antibody titers (Fig. 7D). We conclude that combination of ineffective doses of Fc-Ig1&2 and Fc-mTNFR enables reversal of inflammation, bone damage, and cartilage erosion when administered after onset of established disease, suggesting the potential for pharmacologic synergism between TNF inhibition and PTPRS-targeted therapies for RA treatment.

DISCUSSION

The advent of immunosuppressant DMARDs in the past two decades has undoubtedly revolutionized management of RA. However, an unmet need persists in RA, because immunosuppressant DMARDs increase the risk of infection and a significant fraction of patients still fails to achieve persistent remission despite trying multiple different DMARDs (*4*). Combining current DMARDs with novel agents against FLS targets that are not expressed or irrelevant in immune cells is considered a promising strategy to enhance the efficacy of immunosuppressant DMARDs (*4*). An important indication for FLS-targeting agents would be incomplete response to immunosuppressant DMARDs, because targeting FLS could enhance the effect of anti-cytokine therapeutics by blocking inflammation downstream additional stimuli. However, FLS-targeting therapy could also be useful as a DMARD-sparing strategy in patients experiencing an unacceptable rate/seriousness of infections. Furthermore, RA

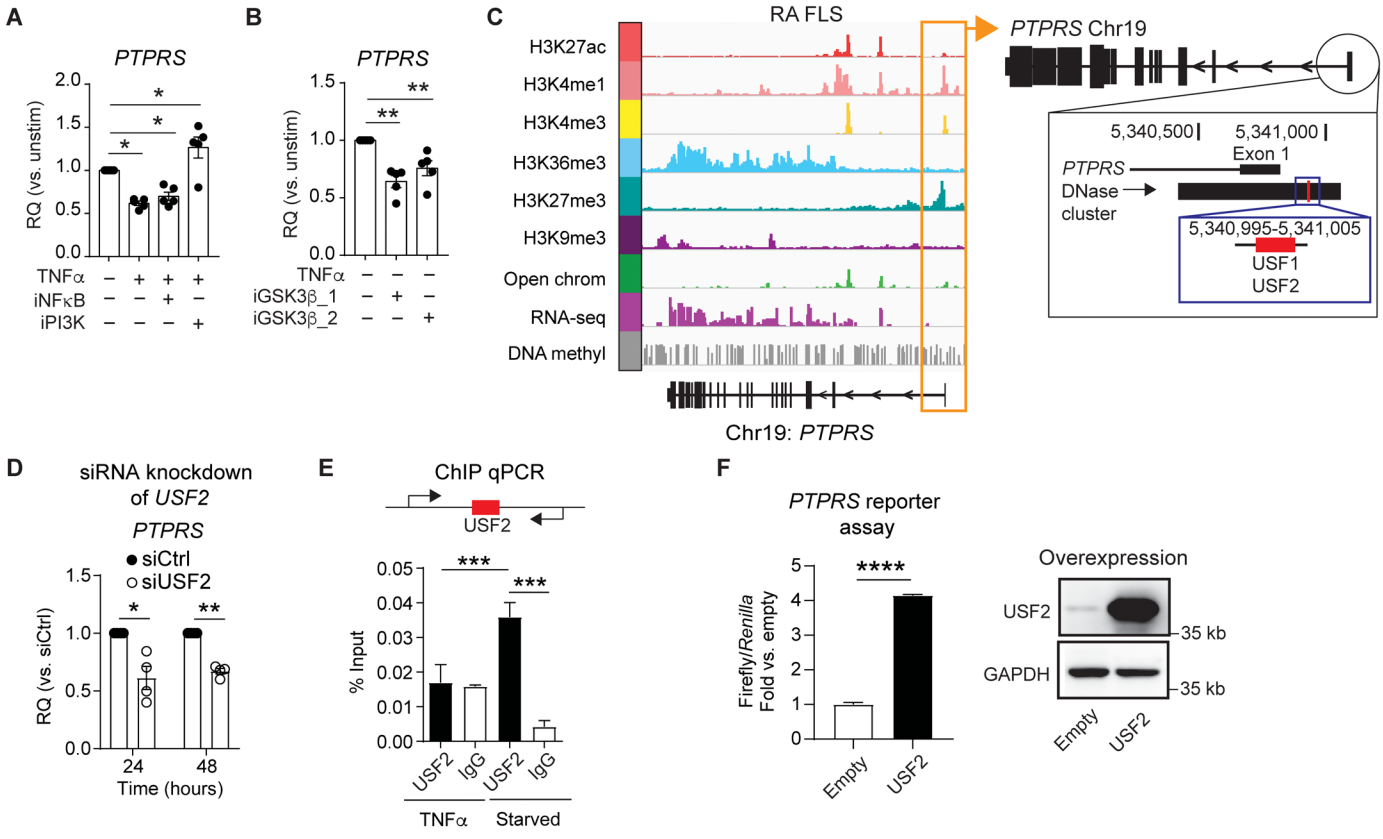

Fig. 6. TNF regulates PTPRS expression in RA FLS through the PI3K/GSK3β/USF2 pathway. (**A** and **B**) Expression of *PTPRS* in RA FLS ($n = 5$) stimulated with TNFα (5 ng/ml) for 12 hours in the presence of NFκB or PI3K inhibitors (A) or after inhibition of GSK3β (B) in serum starved RA FLS ($n = 5$) using two different GSK3β inhibitors. (**C**) Epigenomic landscape of the *PTPRS* locus in one representative RA FLS line. Yellow box indicates *PTPRS* promoter region with highlight of DNase and transcription factor cluster around exon 1 obtained from the UCSC Genome Browser. (**D**) Expression of *PTPRS* in RA FLS ($n = 4$) cultured in normal growth media after transfection with either scrambled (siCtrl) or *USF2*-targeting (siUSF2) siRNA. (**E**) ChIP assay of USF2 binding to the promoter region of *PTPRS*. Representative of three independent experiments ($n = 3$) performed in technical triplicates. (**F**) Luciferase reporter assay of the promoter region of *PTPRS* in HEK293T cells after transfection with empty or USF2 expressing vector. Right panel shows expression of USF2 in transfected HEK293T cells. Representative of two independent experiments ($n = 2$). Graphs represent means ± SEM. *$P < 0.05$, **$P < 0.01$, ***$P < 0.001$, and ****$P < 0.0001$ by one-way ANOVA (E) or paired ratio *t* test (A, B, D, and F) calculated on non-normalized data.

FLS also develop permanent epigenetic modifications that enhance invasiveness (*7*) and might drive smoldering inflammation and cause long-term damage even if a satisfactory clinical response to available DMARDs has been achieved. Thus, targeting FLS might be necessary in a subset of patients to secure permanent or long-term control of disease.

Cadherin-11 is the first validated target for FLS-directed RA therapy (*13*, *37*), and anti–cadherin-11 agents have recently progressed to clinical trials in RA in combination with TNF inhibitors. However, drugging FLS remains in its infancy and, although some DMARDs such as JAK inhibitors have been shown to reduce FLS activation (*12*), very few additional FLS-specific candidate targets have been identified besides cadherin-11 (*4*). In addition, most putative FLS targets lack the key lines of evidence that are needed to fully validate them for anti-FLS/DMARD combination approach in RA. For example, it was only recently demonstrated that FLS play a role in CIA (*10*), and no study of an anti-FLS agent has been reported in CIA or other adaptive immunity–driven RA models. Also, the ideal anti-FLS agent would lack any direct immunomodulation activity, however for none of the currently known FLS targets has a mechanism of action involving innate or adaptive immune cells been rigorously excluded. Perhaps more unexpectedly, no studies of FLS-targeted agents in combination with immunosuppressive DMARDs in models of RA have been reported. Because many critical proteins involved in FLS pathophysiology—including cadherin-11 (*37*)—are induced by arthritogenic cytokines, a preliminary assessment of pharmacological synergies of any new potential FLS target with immunosuppressive DMARDs would be desirable. However, it is currently unknown whether DMARDs influence the expression of cadherin-11 or other therapeutic targets in RA FLS.

Here, by focusing on PTPRS as a candidate target for FLS-directed RA therapy, we provide multiple levels of proof-of-principle evidence that targeting FLS with an anti-PTPRS agent is a viable strategy for RA. First, we show that Ig1&2 potently prevents cartilage and bone damage and reverses inflammation in multiple mouse models of innate and adaptive immunity–driven arthritis. The marked protection from cartilage and bone damage achieved via Ig1&2 monotherapy, coupled with the enrichment of PTPRS in synovial lining FLS, supports the results of a recent report proposing that synovial lining FLS are the main and direct mediators of cartilage damage in RA (*10*) and strongly promote bone erosion via secretion of osteoclast-promoting factors [i.e, RANKL (receptor activator of nuclear factor kappa-B ligand)] and perhaps additional mechanisms (*7*, *10*).

Our bone marrow chimera experiments clearly point to radioresistant cells as the key mediators of Ig1&2 efficacy in arthritis. Low

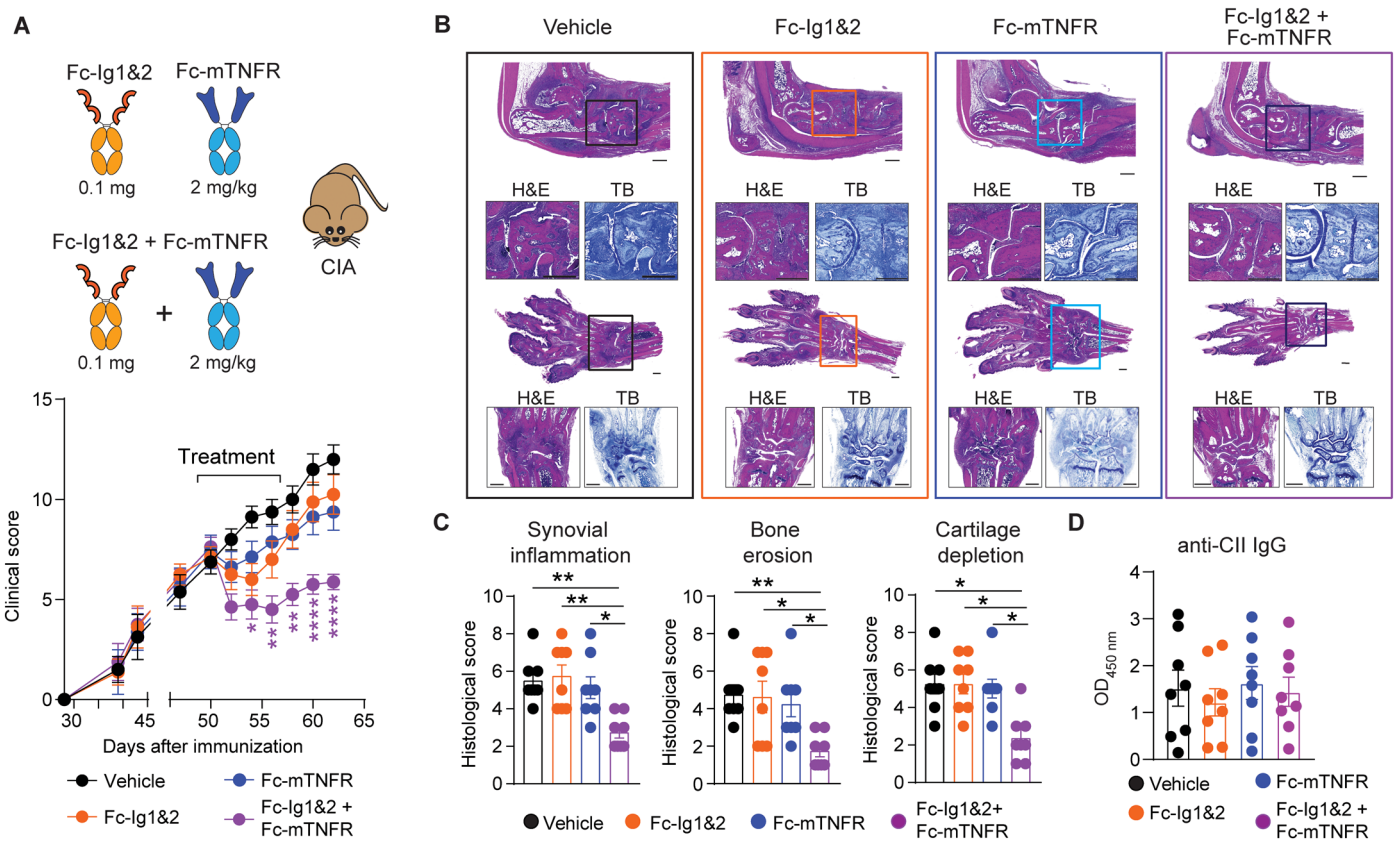

Fig. 7. Therapeutic synergy between Fc-Ig1&2 and Fc-mTNFR in CIA. (**A**) CIA was induced in male DBA/1J mice. Once arthritis was established, mice were treated intraperitoneally with either 0.1 mg of Fc-Ig1&2, Fc-mTNFR (2 mg/kg), combination of 0.1 mg of Fc-Ig1&2 and Fc-mTNFR (2 mg/kg), or vehicle control ($n = 8$ for each treatment group). Arthritis was evaluated by clinical scoring. (**B** and **C**) Representative images of H&E and Toluidine blue (TB) staining (B) used for histopathological evaluation of synovial inflammation, bone erosion, and cartilage depletion (C) in one hind paw and one front paw isolated from mice in (A). Scale bars, 500 μm. (**D**) Serum level of anti-collagen IgG at day 62 from mice in (A). Graphs represent means ± SEM. *$P < 0.05$, **$P < 0.01$, and ****$P < 0.0001$ by two-way ANOVA (A) or Kruskal-Wallis (C).

PTPRS expression levels were detected on joint MHCII$^-$CD64$^+$ tissue-resident macrophages, which are considered radioresistant. However, because MHCII$^-$CD64$^+$ tissue-resident macrophages play an arthritis-protective role (*28*), it is unlikely that they contribute to the therapeutic effect of Ig1&2. Consistent with the previously proposed concept that PTPRS has a very limited and cell-restricted expression in immune cells, we find that PTPRS is not expressed on the vast majority of immune cells, including neutrophils, in arthritic mice. Our in vitro and in vivo assays also did not reveal any significant suppression of T cell, B cell, and/or macrophage function, although additional studies are warranted to rigorously rule out any potential effects on T cell differentiation during early arthritis development. We did confirm that PTPRS is highly expressed in pDCs where it reportedly serves as a critical inhibitor of type 1 interferon (IFN) production (*19*). Type I IFN reportedly plays a protective role in the K/BxN model of arthritis (*38*). However, pDC depletion did not alter the efficacy of Ig1&2 in this model. Further studies are warranted to assess the effect of Ig1&2 on pDCs and on the susceptibility and course of infections in vivo. However, we believe that it is unlikely that Ig1&2 markedly affects type I IFN responses and/or overall causes significant immunosuppression in vivo.

While the high expression of PTPRS on lining FLS likely underlies the effectiveness of Ig1&2 at protecting arthritic mice from cartilage and bone damage, the notable anti-inflammatory effect of Ig1&2 is harder to reconcile with known functions of PTPRS and RA FLS subset features. PTPRS shows low expression in sublining FLS, which are key promoters of immune cell recruitment to inflamed joints (*10*). In addition, Ig1&2 does not influence Toll-like receptor 4 (TLR4)–, IL-1–, and TNF-induced transcriptional responses in RA FLS (*15*). Thus, our data suggest that FLS invasiveness per se triggers additional yet unknown mechanisms that amplify inflammation in autoimmune arthritis. For example, FLS migration might induce release of pro-inflammatory/chemotactic matrix components. This hypothesis warrants further experimental assessment using Ig1&2; however, rigorous testing via genetic manipulation of mice will require the development of approaches—not yet available—to selectively delete lining versus sublining FLS and/or selective genes in FLS.

Although a confirmation of the relationship between PTPRS and TNF expression in additional RA biopsy cohorts is warranted, multiple complementary lines of evidence our study suggest that expression of PTPRS in FLS is regulated by TNF via a novel GSK3β-dependent pathway and induced by TNF inhibition in vivo. We believe that this phenomenon underlies the positive synergy shown when treating arthritic mice with a combination of Fc-mTNFR and Ig1&2 doses that are ineffective alone to reverse arthritis. Thus, we provide here proof-of-principle experimental evidence that treatment of mice

with a combination of an immunosuppressive DMARD and a non-immunosuppressive anti-FLS agent enhances control of disease activity. In addition, we suggest that assessment of synergy between DMARDs and FLS-targeted agents is an important step not only to prioritize combinations with positive synergies but also to rule out negative synergies for agents targeting the potential FLS targets that are induced by inflammatory cytokines.

In conclusion, our study provides the first evidence that a non-immunomodulating anti-FLS approach works well in multiple models of RA and synergizes with TNF blockade in experimental arthritis. A limitation of our study is inherent to the exclusive use of mouse models of RA, which are known to be unable to recapitulate the full pathogenesis of human RA (*39*). Furthermore, the potential variability of PTPRS expression in different patient subsets (e.g., naïve versus treated and DMARD-sensitive versus DMARD-resistant) remains to be established. Nevertheless, we provide for PTPRS a level of validation never achieved so far for a potential target of FLS-directed RA therapy, and we hope that our data will pave the way to further translation of anti-FLS and anti-PTPRS approaches to the clinic.

The notable clinical effectiveness of Ig1&2 when administered alone in CIA suggests that anti-PTPRS agents might be effective as a monotherapy. Although no clinically evident safety signal emerged from our in vivo studies thus far, any potential translation of anti-PTPRS agents will require a thorough assessment of their safety profile. Because even subtherapeutic doses of Ig1&2 could be useful in combination with TNF inhibitors, we believe that development of anti-PTPRS agents as synergistic combinations with TNF blockers would maximize their efficacy/side effects ratio and enhance chances of successful commercialization.

MATERIALS AND METHODS

Preparation of human synovial fluids, FLS lines, and synovial tissues

Synovial fluids were collected before a research synovial biopsy procedure [University of California, San Diego Institutional Review Board (UCSD IRB) protocol no. 160920] by needle aspiration from the knees of three individual patients with RA (RA1, RA2, and RA3; two females and one male), all with anti-CCP-positive RA meeting (American College of Rheumatology/European League against Rheumatism) ACR/EULAR criteria and high-grade synovitis with palpable joint effusions (UCSD IRB protocol no. 140175). The fluids were aliquoted, snap-frozen neat immediately after collection, and used after deidentification.

FLS were obtained from the UCSD Clinical and Translational Research Institute Biorepository and from the Showa University Division of Rheumatology. Each line was previously obtained from discarded synovial tissue from different patients with RA undergoing synovectomy, as described in (*40*). The diagnosis of RA conformed to the ACR 1987 revised criteria (*41*), and the diagnosis of OA conformed to the ACR 1986 or 1991 criteria (*42*, *43*). FLS were collected and used for experiments as approved by the UCSD IRB under protocol no. 140175 and the Showa University School of Medicine IRB under protocol no. 1430 or used for experiments as approved by the La Jolla Institute for Immunology IRB under protocol no. CB-120-0614.

Synovial complementary DNA (cDNA) and synovial tissue specimens from patients with RA were obtained by the William Harvey Research Institute under approved IRB protocol nos. 05/Q0703/198 and 10/H0801/47 (clinical characteristics are reported in fig. S8F). Human synovial tissue specimens used for IF were obtained from patients with RA or OA during joint replacement surgery at the Sahlgrenska University Hospital. The procedures were approved by the Ethics Committee of Gothenburg under protocol no. 573-07. All patients signed consent forms approved by the local IRBs.

FLS were cultured in Dulbecco's modified Eagle's medium (DMEM; Corning) with 10% fetal bovine serum (FBS; Omega Scientific), 2 mM L-glutamine, gentamicin (50 μg/ml), penicillin (100 U/ml), and streptomycin (100 μg/ml) (Life Technologies) at 37°C in a humidified atmosphere containing 5% CO_2. For all experiments, FLS were used between passages 4 and 10, and the cells were synchronized in 0.1% FBS (serum starvation medium) for 24 to 48 hours before experiments unless otherwise noted.

Human dermal fibroblasts

Dermal fibroblast lines from healthy human donors (NHDF) were isolated from skin specimens obtained from the National Disease Research Interchange (NDRI) as described (*44*). NHDF was cultured in the same complete DMEM and conditions as FLS. For all experiments, NHDF was used between passages 3 and 8, and cells were synchronized in serum starved media with 0.1% FBS for 24 hours before analysis or functional assays.

Preparation of mouse FLS lines

Elbow, knee, and ankle joints from 8-week-old BALB/c mice were isolated. Minced tissues were digested in collagenase IV (0.5 mg/ml) in RPMI 1640 for 2 hours at 37°C with gentle agitation and cultured in the same complete DMEM and conditions as human FLS. Murine FLS were used between passages 4 and 10 and synchronized overnight in 0.1% FBS (serum starvation media) before experiments unless otherwise noted.

Synovial fluid stimulations

Confluent human RA FLS were serum starved in DMEM containing 0.1% FBS. FLS were then stimulated with synovial fluids (diluted 1:10 in the media). Cells were harvested for RNA extraction after 12 hours of stimulation. Expression of *PTPRS* and *IL6* was analyzed by qPCR and normalized toward the expression of *GAPDH*.

Assays with signaling inhibitors

RA FLS were serum starved in DMEM containing 0.1% FBS. FLS were then were preincubated with either 0.5 μM NFκB inhibitor Bay 11-7085 (Sigma-Aldrich) or 1 μM PI3K inhibitor LY294002 (Cell Signaling Technology) for 1 hour before stimulation with TNFα (5 ng/ml) for 12 hours. For inhibition of GSK3β, serum starved RA FLS were treated with either 20 μM GSK3β inhibitor SB 415286 (iGSK3β_1; Sigma-Aldrich) or 20 nM GSK3β inhibitor A1070722 (iGSK3β_2; Tocris Bioscience) for 12 hours.

FLS migration assay

Confluent FLS were serum starved for 24 hours in DMEM containing 0.1% FBS, harvested by trypsin digestion, and seeded at 5×10^4 cells in 100 μl of serum-free DMEM containing 0.5% bovine serum albumin (BSA) in the upper chamber of a 6.5-mm-diameter Transwell polycarbonate culture insert with a pore size of 8 μm (Costar). Inserts were placed in 24-well plates with 600 μl of DMEM containing 10% FBS. The assay plates were incubated in presence/absence of Fc-Ig1&2 for 24 hours at 37°C and 5% CO_2, after which the Transwell

inserts were removed, and the upper chamber was gently wiped with a cotton swab to remove nonmigrating cells. Transwell membranes were fixed for 5 min in methanol and stained for 30 min in 0.2% crystal violet in 2% ethanol. Cells were visualized using a Motic AE2000 microscope at 10×. Cells were quantified by counting four nonoverlapping fields using ImageJ software [National Institutes of Health (NIH), version 1.8.0_201]. For migration in the presence of TNF, RA FLS were serum starved for 24 hours and then pretreated with TNF (50 ng/ml) for an additional 24 hours after which cells were seeded as for the migration assay. TNF (50 ng/ml) was also added in combination with Fc-Ig1&2 during the migration assay.

FLS invasion assay

For invasion assays, cells were seeded as for migration assay, except that Corning BioCoat Matrigel Invasion Transwell chambers were used. The assay plates were incubated for 48 hours before staining and imaging as described for migration assay.

For invasion through type I collagen, 8-μm transwells were coated with rat tail type I collagen coating solution (Cell Application Inc., cat. no. 122-20). The solution was diluted in phosphate-buffered saline (PBS) to obtain a final concentration of 30% type I collagen. Inserts were coated with 15 μl (thin gel, 50 μl/cm^2 for a total area of 0.33 cm^2) of a 30% type I collagen solution (0.015 μg/μl), and the matrix was left to polymerize at 37°C for 90 min. Then, 5×10^4 cells were seeded as described for the invasion assay. The assay plates were incubated in the presence/absence of 20 nM Fc-Ig1&2 for 48 hours before staining and imaging as described for the migration assay.

Scratch wound migration assay

RA FLS were grown to confluence in six-well plates and serum starved for 24 hours in DMEM with 0.1% FBS. Cells were scratched with a 1-ml pipette tip and incubated in DMEM containing 1% FBS in the presence of 20 or 40 nM Fc-Ig1&2 or vehicle control. Four images of the wound were captured right after wounding (0 hour) and after 24 hours using a Motic AE2000 microscope at 4× with the software ToupView 3.7. Wound area was calculated using the ImageJ (NIH, version 1.8.0_201) software, and the wound area after 24 hours was normalized to the area at 0 hour.

Proliferation assay

Human RA FLS were harvested and seeded at 7.5×10^3 cells per well in a 96-well plate and serum starved for 24 hours in DMEM containing 0.1% FBS. Then, FLS were allowed to proliferate for 24 hours in response to 10% FBS in DMEM. The CyQUANT NF Cell Proliferation Assay Kit (Invitrogen, cat. no. C35007) was used to measure cellular DNA via fluorescent dye binding according to the manufacturer's instructions. In brief, cells were washed with PBS and then incubated with 100 μl of DNA dye binding solution for 45 min at 37°C. The extent of proliferation was determined by comparing cell counts for samples treated with either 20 nM Fc-Ig1&2 or vehicle. The fluorescence intensity of each sample was measured using a microplate reader with detection at 530 nm.

IF staining of synovial tissue

Paraformaldehyde-fixed paraffin-embedded synovial tissues from RA ($n = 5$) and OA ($n = 4$) (obtained from orthopedic joint replacement surgery) were deparaffinated in xylene rehydrated and subjected to antigen retrieval using citrate buffer in a pressure chamber (2100 Retriever, Aptum Biologics Ltd., Southampton, UK). Nonspecific binding was blocked using serum-free protein block (DAKO). Slides were incubated with mouse monoclonal anti-human PTPRS (1H6, Abnova) and rat anti-human podoplanin (NZ-1, Thermo Fisher Scientific) for 60 min at room temperature, followed by highly cross-absorbed secondary goat anti-mouse/rat Alexa Flour–conjugated antibodies (488/555, respectively). Hoechst was used for nuclear stain. Threshold for positive signal was set by staining with negative control mouse IgG (DAKO). Images were collected on a Zeiss LSM 700 confocal microscope and analyzed with Zen software. Serial tissue sections were subjected to hematoxylin and eosin (H&E) staining for histologic evaluation.

IHC of synovial tissue

Mouse monoclonal anti-human PTPRS antibody was obtained from Abnova, and control IgG antibody (unconjugated goat anti-mouse IgG) was purchased from Vector Laboratories (AI-1000). Paraffin-embedded slides of human RA synovial tissue were deparaffinated in xylene, rehydrated, and pretreated for 10 min with boiling citrate antigen retrieval buffer [1.9 mM citric acid and 10 mM tris-sodium citrate (pH 6.0)] and then treated with 3% H_2O_2 for 10 min to quench endogenous peroxidases. Slides were blocked with 5% goat serum for 1 hour at room temperature and then incubated with anti-PTPRS antibody or control rabbit IgG (1:200 in 5% BSA) overnight at 4°C. Slides were washed and incubated with SignalStain Boost IHC (immunohistochemistry) Detection reagent (Cell Signaling Technology) for 30 min, incubated for 2 min with 3,3′-diaminobenzidine substrate, and counterstained with hematoxylin. Slide images were obtained using an Axio Scan.Z1 slide scanner (Carl Zeiss Microscopy).

Immunoblotting

Cells were lysed in TNE buffer [50 mM tris-HCl (pH 7.5), 150 mM NaCl, and 5 mM EDTA (pH 8.0)] containing 1 mM phenylmethanesulfonyl fluoride, 1× protease inhibitor cocktail (Roche), and PhosSTOP (Sigma-Aldrich). Protein concentration of cell lysates was determined using the Pierce BCA (bicinchoninic acid) Protein Assay Kit (Thermo Fisher Scientific). Immunoblotting was performed using a goat polyclonal anti-human PTPRS antibody (R&D Systems) and a rabbit anti–glyceraldehyde-3-phosphate dehydrogenase (GAPDH) antibody from Cell Signaling Technology.

Quantitative real-time RT-PCR

RNA was extracted using the RNeasy kit (Qiagen). cDNA was synthesized using the SuperScript III First-Strand Synthesis SuperMix for real-time quantitative reverse transcription PCR (qRT-PCR) (Life Technologies). qPCR was performed on a Bio-Rad CFX384 Real-Time PCR Detection System, with primer assays and SYBR Green qPCR Master Mix from SABiosciences/Qiagen. Primer assay efficiencies were guaranteed by the manufacturer to be greater than 90%. Each reaction was measured using technical triplicates, and data were normalized to the expression levels of the housekeeping gene *GAPDH*. Results are presented as fold change compared to either the expression level in control samples with the ΔΔCq method or as fold change compared to the expression of *GAPDH*.

Mice

All animal experiments were carried out in accordance with the Institutional Animal Care and Use Committee–approved protocol (no. AP140-NB4-0610) at the La Jolla Institute for Immunology and UCSD (no. S16098). PTPRS KO mice on a BALB/c background were

generated as previously described in (*45*). DBA/1J (JAX 000670, DBA/1J), BALB/c (JAX 000651, BALB/cJ), and CD45.1 BALB/c [JAX 006584, CByJ.SJL(B6)-Ptprca/J] were obtained from the Jackson laboratory. BALB/c Rag2-KO mice were obtained from Taconic (model 601). KRN mice on the C57BL/6 background were a gift from C. Benoist (Harvard University). Nonobese diabetic (NOD) mice were obtained from Taconic.

Arthritis models

KRN and NOD mice were crossed to obtain offspring that developed arthritis at around 6 to 7 weeks of age (spontaneous K/BxN mice). Serum from arthritic K/BxN mice was pooled for use in the K/BxN STIA model (*27*). To elicit STIA, 6- to 8-week-old mice were injected intraperitoneally with 100 μl of arthritogenic K/BxN serum. Severity of arthritis was evaluated by clinical scoring (as described below) and measurement of ankles swelling every other day, starting on the day of serum injection.

The CIA model was performed as described in (*46*). Briefly, 8- to 10-week-old male DBA/1J mice were immunized with 100 μg of chicken type II collagen (Chondrex) emulsified in Freund's adjuvant containing 50 μg of *Mycobacterium tuberculosis* [H37Ra; American Type Culture Collection (ATCC) 25177] [CFA (complete Freund's adjuvant), Sigma-Aldrich]. After 28 days, mice were boosted with 100 μg of chicken type II collagen emulsified in incomplete Freund's adjuvant (Sigma-Aldrich). In all models, arthritis was clinically scored in wrists and ankles as previously described (*15*): 0 = normal; 1 = minimal erythema and mild swelling; 2 = moderate erythema and mild swelling; 3 = marked erythema and severe swelling, digits not yet involved; and 4 = maximal erythema and swelling, digits involved.

In vivo administration of His-Ig1&2, Fc-Ig1&2, and Fc-mTNFR

Preparation of recombinant PTPRS 6xHisIg1&2 (here called His-Ig1&2) is described in (*15*). Preparation of human IgG1-Fc–fused Ig1&2 (here called Fc-Ig1&2) was contracted to LakePharma (USA). Murine TNF-blocking biologic p75TNFR:Fc (Fc-mTNFR) was obtained from Amgen through the Amgen Extramural Research Alliance Program. His-Ig1&2 in tris-buffered saline (TBS) or vehicle control (TBS), Fc-Ig1&2 in 20 mM tris with 120 mM NaCl or human IgG1-Fc control, and Fc-mTNFR was administered according to the schedule described in the figure legends.

In vivo pDC depletion

pDCs were depleted in mice by two administrations of 500 μg of anti–PDCA-1 (InVivoMAb anti-mouse CD317; BioXCell) or IgG isotype control (BioXCell) by intraperitoneal or retro-orbital (r.o.) injection 2 days apart.

Measurement of serum anti-collagen antibody levels

Anti-collagen antibody levels in sera of mice immunized with collagen were measured by enzyme-linked immunosorbent assay as described (*46*). Briefly, low-binding 96-well multi-well plates (Costar) were coated with type II chicken sternal collagen (1 μg/ml; Sigma-Aldrich). Sera were incubated in serial dilutions, and IgG binding to collagen was detected using a biotinylated anti-mouse IgG antibody (Jackson ImmunoResearch) as well as anti-mouse IgG1, IgG2a, IgG2b, and IgG3 antibodies (SouthernBiotech), followed by incubation with extravidin–horseradish peroxidase (Sigma-Aldrich) and exposure with 3,3′,5,5′-tetramethylbenzidine (TMB) substrate. Plate absorbance was read at 450 nm using a Tecan Infinite M1000 plate reader.

Histological scoring of mouse arthritic joints

Whole hind paws were fixed in 10% formalin, decalcified, trimmed, and embedded. Sections were prepared from tissue blocks and stained with H&E, Safranin O, or Toluidine blue by HistoTox Labs. Histopathological scoring was performed as described (*15*). Briefly, joints of arthritic mice were assigned scores of 0 to 4 for inflammation based on H&E staining, according to the following criteria: 0 = normal; 1 = minimal infiltration of inflammatory cells in periarticular area; 2 = mild infiltration; 3 = moderate infiltration; and 4 = marked infiltration. Joints of arthritic mice were given scores of 0 to 4 for bone resorption based on H&E staining, according to the following criteria: 0 = normal; 1 = minimal (small areas of resorption, not readily apparent on low magnification); 2 = mild (more numerous areas of resorption, not readily apparent on low magnification, in trabecular or cortical bone); 3 = moderate (obvious resorption of trabecular and cortical bone, without full thickness defects in the cortex; loss of some trabeculae; lesions apparent on low magnification); and 4 = marked (full-thickness defects in the cortical bone and marked trabecular bone loss). Cartilage depletion was identified by diminished Safranin O or Toluidine blue staining of the matrix and was scored on a scale of 0 to 4, where 0 = no cartilage destruction (full staining with Safranin O or Toluidine blue), 1 = localized cartilage erosions, 2 = more extended cartilage erosions, 3 = severe cartilage erosions, and 4 = depletion of entire cartilage. Histologic analyses were performed in a blinded manner. Images of whole ankles were acquired using a Zeiss Axioscan.Z1 (Zeiss) slide scanner and analyzed using Zen software (Zeiss).

Micro–computed tomography analysis

Mouse ankles were placed in 10% neutral-buffered formalin. After fixation, samples were transferred to 70% ethanol. Before scanning, bones were transferred to PBS for 48 hours. Scanning was performed on a Skyscan1176 Micro-CT (Bruker) with a voxel size of 9 μm, at 50 kV/200 mA, with a 0.5-mm aluminum filter. Exposure time was 810 ms. The x-ray projections were obtained at 0.4° intervals with a scanning angular rotation of 180° and a combination of four average frames. The projection images were reconstructed into three-dimensional images using NRecon software (Bruker) and DataViewer (Bruker). Data were processed using CT-Analyzer software (Bruker), and images were generated using CTVOX software (Bruker). Bone erosion was quantified as described in (*46*).

Radiolabeling of Fc-Ig1&2 and Fc-mTNFR

To allow for radiolabeling, the agents were first functionalized with DOTA (tetraxetan) to provide chelation sites to attach the radioactive atom. To covalently couple Fc-Ig1&2 to DOTA, typically, 0.8 mg of protein was immobilized on 0.5 ml of heparin-agarose beads (Sigma-Aldrich) in a total of 1.3 ml of tris (pH 7.3) and 150 mM NaCl. DOTA–*N*-hydroxysuccinimide ester (Macrocyclics) was added at a concentration of 0.77 mM and incubated at room temperature for 30 min. After extensive washing in the same buffer, the protein was eluted in 750 mM NaCl and 20 mM tris (pH 8.3), further purified by size exclusion chromatography (Bio-Rad SEC 650) and concentrated to 12 to 15 mg/ml. Fc-mTNFR was modified in a similar way, except that no immobilization on solid support was necessary. The reaction was routinely monitored by Native polyacrylamide gel electrophoresis.

Following this functionalization step, the conjugates were incubated with ^{111}In for 3 hours at 43°C and purified through a P10 separation column.

Biodistribution studies

STIA was induced in BALB/c mice by an intraperitoneal injection of 100 μl of K/BxN serum, as described under arthritis models. Injection of radiolabeled proteins and subsequent imaging began at the peak of arthritis, which occurs 8 days after serum injection. All animals were anesthetized with isoflurane before injections and imaging. Each animal received an intravenous injection of radiolabeled agent, with a dose of approximately 170 μCi per animal. Four arthritic mice were injected with approximately 170 μCi of ^{111}In-labeled Fc-Ig1&2 and compared with five arthritic mice injected with 280 μCi of ^{111}In-labeled Fc-mTNFR. Immediately after injection, each animal was loosely restrained on the surface of the γ-Imager planar gamma imaging system (Biospace Lab, Nesles la Vallée, France), with continued anesthesia. The animals were placed on their backs with paws loosely taped to the top of the imager and the ^{111}In collimator in place. Each animal was imaged for 10 min at 1 and 6 hours and 1, 3, and 5 days after injection. Each image also included a standard with 5% of the injected dose, placed as a point source next to the animal. Following the final image, the mice were sacrificed; and samples were collected of blood, bladder, liver, kidney, spleen, heart, lung, brain, eye, and paws into plastic scintillation vials, weighed; and the activity in each vial was measured in a Gamma 9000 gamma counter (Beckman Coulter, Brea, CA). Images were analyzed with GammaVision software, calculations were performed in Excel, and graphs were constructed in SigmaPlot. Regions of interest (ROIs) were drawn around the hind paws and the standard at each time point. Total counts and ROI area were recorded for each ROI and exported into Excel. There, all the counts were corrected for decay, and the total counts for each ROI were divided by the ROI area to provide a value of signal/area for each paw and the standard. All the values for the standards were normalized to 5%. This produced a correction factor that allowed all paw values to be converted from raw counts into percent of injected dose. The percent of injected dose of both hind paws at each time point was averaged together, and the resulting values were then averaged across all mice at each time point and plotted. Gamma counter values for each organ were used to calculate the percent of injected dose per organ uptake at day 5. A value of 72 ml/kg of blood was used to calculate the total volume and thus total signal for blood in each animal, from a smaller quantity collected at sacrifice. These percent of the injected dose per organ values were also compared and plotted across each mouse group.

Flow cytometry

Single-cell suspensions were prepared from lymph nodes and spleen. For isolation of cells from mouse blood, blood was collected into 2 mM EDTA in PBS via r.o. bleed (from live animals) or cardiac puncture (from euthanized animals). Erythrocytes were lysed from spleen and mouse blood using eBiosience red blood cell lysis buffer (Thermo Fisher Scientific). For isolation of synovial cells, ankle joints were collected, and the tibia and digits disarticulated by pulling with blunt forceps and bone marrow flushed out to avoid bone marrow contamination. Joints were rinsed with PBS and dissociated with Liberase (Roche) and deoxyribonuclease I (DNase I) at 37°C for 60 min. Cells were preincubated with Fc block (BD Pharmingen) before antibody staining. For surface staining, fluorochrome-conjugated antibodies specific for CD3 (17A2), CD19 (6D5), NK1.1 (PK136), CD11b (M1/70), CD44 (IM7), Ly6G (1A8), Ly6C (HK1.4), CD45.1 (A20), MHCII (M5/114.15.2), CD64 (X54-5/7.1), and CD115 (AFS98) were obtained from BioLegend. CD43 (R2/60), PD1 (RMP1-30), GL7 (GL-7), CD25 (PC61.5), B220 (RA3-6B2), CD317/BST2 (eBio927), CD62L (MEL-14), CD45.2 (104), TCR-β (T cell receptor–β) (H57-597), CD8 (53-6.7), and CD4 (RM4-5) were obtained from eBioscience/Thermo Fisher Scientific. For intracellular cytokine staining, cells were incubated with phorbol 12-myristate 13-acetate (PMA; 20 ng/ml; Sigma-Aldrich) and 1 μm ionomycin (Sigma-Aldrich) in the presence of brefeldin A (3 μg/ml; eBioscience/Thermo Fisher Scientific) for 5 hours at 37°C. Intracellular staining was performed with the intracellular fixation buffer (eBioscience/Thermo Fisher Scientific) and permeabilization buffer (eBioscience/Thermo Fisher Scientific). For intracellular staining of transcription factors, the FoxP3/Transcription Factor Staining Buffer Set was used (eBioscience/Thermo Fisher Scientific). Antibodies recognizing FoxP3 (FJK-16s), IL-17A (eBio17B7), and IFNγ (XMG1.2) were obtained from eBioscience/Thermo Fisher Scientific, and BCL6 was obtained from BD Biosciences. Dead cells were excluded from analysis by staining with Fixable Viability dye from eBioscience/Thermo Fisher Scientific.

Data were acquired on a ZE5 flow cytometer (Bio-Rad) equipped with Everest Software. Analysis was performed using FlowJo software (TreeStar). Cell sorting was performed on a FACSAria III instrument (BD Biosciences). For flow analysis, anti-mouse PTPRS (MédiMabs) was labeled with Alexa Fluor 647 using Mix-n-Stain antibody labeling kit (Sigma-Aldrich).

Bone marrow reconstitution

To generate bone marrow chimeras, male BALB/cByJ (CD45.1 congenic) mice were lethally irradiated with two doses of 5.5 Gy using an RS 2000 Biological irradiator and subsequently administered bone marrow from male PTPRS WT or KO congenic CD45.2 donor mice. KBxN serum was administered to induce arthritis 8 weeks after irradiation. After 7 weeks, chimerism was verified by flow cytometry by staining for the appropriate CD45 allele (anti-CD45.1 and anti-CD45.2; eBioscience). The percentage of engraftment in recipient mice was greater than 95%.

M1 and M2 polarization of BMDMs

Bone marrow cells were isolated from 8- to 12-week-old BALB/c mice. Total bone marrow cells were plated in six-well culture plates (2×10^6 cells per well) in complete IMDM (Iscove's Modified Dulbecco's Medium) media containing 10% FBS, 25 mM Hepes, 2 mM L-glutamine, penicillin (100 U/ml), streptomycin (100 μg/ml), and macrophage colony-stimulating factor (M-CSF; 20 ng/ml) (BioLegend). Nonadherent cells were removed after 24 hours by washing with PBS and replacing with new complete IMDM media containing M-CSF (20 ng/ml). Media was replaced every 3 days, and cells were cultured for a total of 7 days. After 7 days, BMDMs were left unstimulated (M0) or stimulated with either lipopolysaccharide (100 ng/ml; Sigma-Aldrich) and IFNγ (50 ng/ml; BioLegend) for M1 polarization or IL-4 (10 ng/ml; BioLegend) and IL-13 (10 ng/ml; BioLegend) for M2 polarization. Fc-Ig1&2 (20, 40, and 80 nM) was added to the cells during polarization. Cells were collected after 24 hours, and RNA was extracted using the RNeasy Micro Kit (Qiagen). Expression of M1-related genes *Tnf*, *Il1b*, *Nos2*, and *Il12* and M2-related genes *Pparg*, *Arg1*, *Retnla*, and *Mrc1* were analyzed by qPCR. Expression was normalized to the expression of *Gapdh*.

Phagocytosis assay

Bone marrow cells were isolated from 8- to 12-week-old BALB/c mice and cultured in 12-well plates (1×10^6 cells per well) under BMDM conditions as described above. After 7 days, BMDMs were either left unstimulated (M0 condition) or under M1- or M2-polarizing conditions as described above. Fc-Ig1&2 (20, 40, or 80 nM) was added during M1 and M2 polarization. After 24 hours, polarizing media was replaced with IMDM without FBS, and cells were cultured for 1 hour in the presence of either Fc-Ig1&2 (20, 40, or 80 nM) or vehicle control for 1 hour. After 1 hour, either pHrodo Red *E. coli* or pHrodo Green *S. aureus* BioParticles (Invitrogen) were added to the cells according to the manufacturer's protocol. Cells were allowed to phagocytose bioparticles for 30 min, after which cells were washed, detached from plates using TrypLE Express (Thermo Fisher Scientific), stained with Fixable Viability Dye 780 (Thermo Fisher Scientific), and analyzed by flow cytometry. Cells incubated with bioparticles on ice were used as negative control for phagocytosis. The pH-sensitive dye pHrodo is nonfluorescent at neutral pH but fluoresces brightly upon the acidification that occurs in the phagosome.

CD4 T cell differentiation assays

Naïve CD4 T cells were isolated from pooled spleen and lymph nodes of either 8- to 12-week-old BALB/c or DBA/1J mice using the EasySep Mouse Naïve $CD4^+$ T cell isolation kit (STEMCELL Technologies). Isolated naïve CD4 T cells were polarized into either T_H1, T_H17, or iT_{regs} (induced regulatory T cells) in the presence of Fc-Ig1&2 (20, 40, or 80 nM) or vehicle control using the below described conditions.

For differentiation of T_H1 cells, 1×10^5 naïve CD4 T cells were cultured on anti-CD3 (145-2C11, BioLegend; 2 μg/ml)–coated plates in complete RPMI 1640 media [10% FBS, penicillin (100 U/ml), streptomycin (100 μg/ml), 1× nonessential amino acids, 25 mM Hepes, 55 μM β-mercaptoethanol, and 2 mM L-glutamine] containing soluble anti-CD28 (37.51, BioLegend; 0.5 μg/ml), anti–IL-4 (11B11, BioLegend; 10 μg/ml), recombinant mouse IL-12 (R&D Systems; 25 ng/ml), and recombinant mouse IL-2 (R&D Systems; 25 ng/ml). For differentiation of T_H17 cells, 1×10^5 naïve CD4 T cells were cultured on anti-CD3 (145-2C11; 2 μg/ml)–coated plates in complete RPMI 1640 media containing soluble anti-CD28 (37.51; 1 μg/ml), anti-IFNγ (XMG1.2, BioLegend; 10 μg/ml), anti–IL-4 (11B11, 10 μg/ml), recombinant human transforming growth factor–β1 (TGFβ1) (R&D Systems; 5 ng/ml), and recombinant mouse IL-6 (BioLegend; 50 ng/ml). For iT_{reg} differentiation, 1×10^5 naïve CD4 T cells were cultured on anti-CD3 (145-2C11; 2 μg/ml)–coated plates in complete RPMI 1640 media containing soluble anti-CD28 (37.51; 0.5 μg/ml) and recombinant human TGFβ1 (R&D Systems; 5 ng/ml). Cells were cultured under T_H-polarizing conditions for 5 days. To verify T_H1 and T_H17 differentiation, cells were stimulated with PMA (20 ng/ml) and ionomycin (1 μM) in the presence of brefeldin A (Thermo Fisher Scientific; 3 μg/ml) for 4 hours and analyzed by flow cytometry for the expression of IFNγ and IL-17A. To verify iT_{reg} differentiation, cells were analyzed by flow cytometry for the expression of FoxP3. Cells cultured without polarizing conditions (T_H0) were used as control for polarization.

In a second experiment, we performed polarization of naïve CD4 T cells in the presence of APCs. Naïve CD4 T cells (1×10^5), isolated from BALB/c mice, were cultured with 1×10^5 irradiated BALB/c Rag2-KO splenocytes (35 Gy) as APCs and soluble anti-CD3 (145-2C11, BioLegend; 5 μg/ml) under T_H1-, T_H17-, or iT_{reg}-polarizing conditions. The same polarizing conditions as described above were used; however, soluble anti-CD28 was removed because of the presence of irradiated APCs. Differentiation of T_H1, T_H17, and iT_{regs} was verified as described above.

Epigenetic evaluation of the *PTPRS* and *SDC4* loci

Data used for evaluation of the epigenetic and transcriptomic landscape in the *PTPRS* and *SDC4* loci in RA (n = 10 lines) and OA (n = 10 lines) FLS were obtained as described previously (*23*). Data are available in the Gene Expression Omnibus with the primary accession code GSE112658. Images were generated using Integrative Genomics Viewer version 2.3.98. USF2-binding sites in the *PTPRS* promoter region were identified using the UCSC Genome Browser (GRCh37/hg19) together with the Transcription Factor ChIP sequencing clusters from ENCODE (version March 2012) and DNase I Hypersensitivity Clusters from ENCODE (V3).

Transfection and dual-luciferase reporter assay

Dual-luciferase assays were performed in human embryonic kidney (HEK) 293T cells obtained from the ATCC. Confluent HEK293T cells were transfected using polyethylenimine (PEI) in a ratio of 3 to 1 per μg of plasmid in Opti-MEM. Overexpression vector for human USF2 or an empty control vector was obtained from VectorBuilder Inc. A luciferase promoter region reporter vector containing a 120–base pair portion of the *PTPRS* promoter region (UCSC Genome Browser on Human GRCh37/hg19 position: chr19:5,340,976-5,341,095) containing binding sites for USF2 was obtained from VectorBuilder Inc. Cells were incubated for 24 hours after transfection. Luciferase activity was assessed using the Dual-Luciferase Reporter Assay System from Promega according to the manufacturer's protocol. *Renilla* luciferase activity was used to normalize firefly luciferase activity.

Chromatin immunoprecipitation

RA FLS were cultured to confluency, serum starved for 24 hours, and stimulated with recombinant human TNFα (50 ng/ml) for 6 hours or left unstimulated. Then, cells were fixed in 1% formaldehyde for 15 min at room temperature. After sonication, chromatin was immunoprecipitated with the Pierce Magnetic ChIP assay Kit (Thermo Fisher Scientific) using a rabbit anti-USF2 antibody (NBP2-56717, Novus Biologicals) overnight at 4°C according to the manufacturer's instructions. The eluted DNA was used for *PTPRS* promoter region PCR and qPCR. Ten percent input for each condition was used for normalization. Human *PTPRS* promoter primers, 5′-TCTGCCCCGCTTCACATCG-3′ (forward) and 5′-AGCCGCCACCACCACCACCA-3′ (reverse), were purchased from Integrated DNA Technologies and used for ChIP qPCR with the PowerUp SYBR Green PCR Master Mix (Thermo Fisher Scientific) and PCR using the OneTaq Hot Start Quick-Load 2× Master Mix with GC buffer (New England Biolabs Inc.).

siRNA-mediated knockdown

RA FLS were grown to confluency (70%) and transfected with 1 μg of ON-TARGETplus SMARTpool siRNA-targeting human *USF2* (Dharmacon) or 1 μg of ON-TARGETplus Nontargeting Pool siRNA (Dharmacon) using the Human Dermal Fibroblast Nucleofector Kit (Lonza) according to the manufacturer's protocol. In brief, 5×10^5 RA FLS were resuspended in 100 μl of nucleofector solution containing siRNA and electroporated with program U-23 on an

Amaxa Nucleofector II. Transfected cells were divided into three individual wells in a six-well plate. Cells were harvested for RNA extraction after 24 and 48 hours, and expression of *USF2* and *PTPRS* was analyzed by qPCR and normalized toward the expression of *GAPDH* as described above. Fold change in expression was calculated against the expression in RA FLS treated with control siRNA using the ΔΔ*C*T method.

Statistical analysis

Sample sizes were selected on the basis of our experience with the assays being performed to achieve sufficient power to detect biologically relevant differences in the experiments being conducted. The two- or one-way analysis of variance (ANOVA), Spearman correlation, Kruskal-Wallis, paired or unpaired *t* test, paired ratio *t* test, and Mann-Whitney *U* test were performed where appropriate as reported in the figure legends. Parametric tests were only used on normally distributed variables as assessed by the Shapiro-Wilk test. All statistical analyses were performed using GraphPad Prism software. A comparison was considered significant if *P* was less than 0.05.

SUPPLEMENTARY MATERIALS

Supplementary material for this article is available at http://advances.sciencemag.org/cgi/content/full/6/26/eaba4353/DC1

View/request a protocol for this paper from *Bio-protocol*.

REFERENCES AND NOTES

1. I. B. McInnes, G. Schett, The pathogenesis of rheumatoid arthritis. *N. Engl. J. Med.* **365**, 2205–2219 (2011).
2. M. K. Demoruelle, K. D. Deane, Treatment strategies in early rheumatoid arthritis and prevention of rheumatoid arthritis. *Curr. Rheumatol. Rep.* **14**, 472–480 (2012).
3. B. Jarvis, D. Faulds, Etanercept: A review of its use in rheumatoid arthritis. *Drugs* **57**, 945–966 (1999).
4. M. Feldmann, R. N. Maini, Perspectives from masters in rheumatology and autoimmunity: Can we get closer to a cure for rheumatoid arthritis? *Arthritis Rheumatol.* **67**, 2283–2291 (2015).
5. A. Richter, J. Listing, M. Schneider, T. Klopsch, A. Kapelle, J. Kaufmann, A. Zink, A. Strangfeld, Impact of treatment with biologic DMARDs on the risk of sepsis or mortality after serious infection in patients with rheumatoid arthritis. *Ann. Rheum. Dis.* **75**, 1667–1673 (2016).
6. M. C. Genovese, S. Cohen, L. Moreland, D. Lium, S. Robbins, R. Newmark, P. Bekker; 20000223 Study Group, Combination therapy with etanercept and anakinra in the treatment of patients with rheumatoid arthritis who have been treated unsuccessfully with methotrexate. *Arthritis Rheum.* **50**, 1412–1419 (2004).
7. N. Bottini, G. S. Firestein, Duality of fibroblast-like synoviocytes in RA: Passive responders and imprinted aggressors. *Nat. Rev. Rheumatol.* **9**, 24–33 (2013).
8. S. Lefevre, A. Knedla, C. Tennie, A. Kampmann, C. Wunrau, R. Dinser, A. Korb, E.-M. Schnäker, I. H. Tarner, P. D. Robbins, C. H. Evans, H. Stürz, J. Steinmeyer, S. Gay, J. Schölmerich, T. Pap, U. Müller-Ladner, E. Neumann, Synovial fibroblasts spread rheumatoid arthritis to unaffected joints. *Nat. Med.* **15**, 1414–1420 (2009).
9. E. Neumann, S. Lefèvre, B. Zimmermann, S. Gay, U. Müller-Ladner, Rheumatoid arthritis progression mediated by activated synovial fibroblasts. *Trends Mol. Med.* **16**, 458–468 (2010).
10. A. P. Croft, J. Campos, K. Jansen, J. D. Turner, J. Marshall, M. Attar, L. Savary, C. Wehmeyer, A. J. Naylor, S. Kemble, J. Begum, K. Dürholz, H. Perlman, F. Barone, H. M. McGettrick, D. T. Fearon, K. Wei, S. Raychaudhuri, I. Korsunsky, M. B. Brenner, M. Coles, S. N. Sansom, A. Filer, C. D. Buckley, Distinct fibroblast subsets drive inflammation and damage in arthritis. *Nature* **570**, 246–251 (2019).
11. S. G. Dakin, M. Coles, J. P. Sherlock, F. Powrie, A. J. Carr, C. D. Buckley, Pathogenic stromal cells as therapeutic targets in joint inflammation. *Nat. Rev. Rheumatol.* **14**, 714–726 (2018).
12. S. Rosengren, M. Corr, G. S. Firestein, D. L. Boyle, The JAK inhibitor CP-690,550 (tofacitinib) inhibits TNF-induced chemokine expression in fibroblast-like synoviocytes: Autocrine role of type I interferon. *Ann. Rheum. Dis.* **71**, 440–447 (2012).
13. D. M. Lee, H. P. Kiener, S. K. Agarwal, E. H. Noss, G. F. M. Watts, O. Chisaka, M. Takeichi, M. B. Brenner, Cadherin-11 in synovial lining formation and pathology in arthritis. *Science* **315**, 1006–1010 (2007).
14. S. K. Chang, E. H. Noss, M. Chen, Z. Gu, K. Townsend, R. Grenha, L. Leon, S. Y. Lee, D. M. Lee, M. B. Brenner, Cadherin-11 regulates fibroblast inflammation. *Proc. Natl. Acad. Sci. U.S.A.* **108**, 8402–8407 (2011).
15. K. M. Doody, S. M. Stanford, C. Sacchetti, M. N. D. Svensson, C. H. Coles, N. Mitakidis, W. B. Kiosses, B. Bartok, C. Fos, E. Cory, R. L. Sah, R. Liu-Bryan, D. L. Boyle, H. A. Arnett, T. Mustelin, M. Corr, J. D. Esko, M. L. Tremblay, G. S. Firestein, A. R. Aricescu, N. Bottini, Targeting phosphatase-dependent proteoglycan switch for rheumatoid arthritis therapy. *Sci. Transl. Med.* **7**, 288ra276 (2015).
16. C. H. Coles, Y. Shen, A. P. Tenney, C. Siebold, G. C. Sutton, W. Lu, J. T. Gallagher, E. Y. Jones, J. G. Flanagan, A. R. Aricescu, Proteoglycan-specific molecular switch for RPTPσ clustering and neuronal extension. *Science* **332**, 484–488 (2011).
17. Y. Shen, A. P. Tenney, S. A. Busch, K. P. Horn, F. X. Cuascut, K. Liu, Z. He, J. Silver, J. G. Flanagan, PTPσ is a receptor for chondroitin sulfate proteoglycan, an inhibitor of neural regeneration. *Science* **326**, 592–596 (2009).
18. S. M. Stanford, M. F. Maestre, A. M. Campbell, B. Bartok, W. B. Kiosses, D. L. Boyle, H. A. Arnett, T. Mustelin, G. S. Firestein, N. Bottini, Protein tyrosine phosphatase expression profile of rheumatoid arthritis fibroblast-like synoviocytes: A novel role of SH2 domain-containing phosphatase 2 as a modulator of invasion and survival. *Arthritis Rheum.* **65**, 1171–1180 (2013).
19. A. Bunin, V. Sisirak, H. S. Ghosh, L. T. Grajkowska, Z. E. Hou, M. Miron, C. Yang, M. Ceribelli, N. Uetani, L. Chaperot, J. Plumas, W. Hendriks, M. L. Tremblay, H. Häcker, L. M. Staudt, P. H. Green, G. Bhagat, B. Reizis, Protein tyrosine phosphatase PTPRS is an inhibitory receptor on human and murine plasmacytoid dendritic cells. *Immunity* **43**, 277–288 (2015).
20. A. R. Aricescu, I. W. McKinnell, W. Halfter, A. W. Stoker, Heparan sulfate proteoglycans are ligands for receptor protein tyrosine phosphatase σ. *Mol. Cell. Biol.* **22**, 1881–1892 (2002).
21. A.-K. Ekwall, T. Eisler, C. Anderberg, C. Jin, N. Karlsson, M. Brisslert, M. I. Bokarewa, The tumour-associated glycoprotein podoplanin is expressed in fibroblast-like synoviocytes of the hyperplastic synovial lining layer in rheumatoid arthritis. *Arthritis Res. Ther.* **13**, R40 (2011).
22. F. Mizoguchi, K. Slowikowski, K. Wei, J. L. Marshall, D. A. Rao, S. K. Chang, H. N. Nguyen, E. H. Noss, J. D. Turner, B. E. Earp, P. E. Blazar, J. Wright, B. P. Simmons, L. T. Donlin, G. D. Kalliolias, S. M. Goodman, V. P. Bykerk, L. B. Ivashkiv, J. A. Lederer, N. Hacohen, P. A. Nigrovic, A. Filer, C. D. Buckley, S. Raychaudhuri, M. B. Brenner, Functionally distinct disease-associated fibroblast subsets in rheumatoid arthritis. *Nat. Commun.* **9**, 789 (2018).
23. R. Ai, T. Laragione, D. Hammaker, D. L. Boyle, A. Wildberg, K. Maeshima, E. Palescandolo, V. Krishna, D. Pocalyko, J. W. Whitaker, Y. Bai, S. Nagpal, K. E. Bachman, R. I. Ainsworth, M. Wang, B. Ding, P. S. Gulko, W. Wang, G. S. Firestein, Comprehensive epigenetic landscape of rheumatoid arthritis fibroblast-like synoviocytes. *Nat. Commun.* **9**, 1921 (2018).
24. A. Barski, S. Cuddapah, K. Cui, T. Y. Roh, D. E. Schones, Z. Wang, G. Wei, I. Chepelev, K. Zhao, High-resolution profiling of histone methylations in the human genome. *Cell* **129**, 823–837 (2007).
25. R. O. Williams, Collagen-induced arthritis as a model for rheumatoid arthritis. *Methods Mol. Med.* **98**, 207–216 (2004).
26. C. A. Notley, J. J. Inglis, S. Alzabin, F. E. McCann, K. E. McNamee, R. O. Williams, Blockade of tumor necrosis factor in collagen-induced arthritis reveals a novel immunoregulatory pathway for Th1 and Th17 cells. *J. Exp. Med.* **205**, 2491–2497 (2008).
27. P. A. Monach, D. Mathis, C. Benoist, The K/BxN arthritis model. *Curr Protoc Immunol* **Chapter 15**, Unit 15 22 (2008).
28. A. V. Misharin, C. M. Cuda, R. Saber, J. D. Turner, A. K. Gierut, G. K. Haines III, S. Berdnikovs, A. Filer, A. R. Clark, C. D. Buckley, G. M. Mutlu, G. R. S. Budinger, H. Perlman, Nonclassical Ly6C$^-$ monocytes drive the development of inflammatory arthritis in mice. *Cell Rep.* **9**, 591–604 (2014).
29. L. W. Kaminsky, J. J. Sei, N. J. Parekh, M. L. Davies, I. E. Reider, T. E. Krouse, C. C. Norbury, Redundant function of plasmacytoid and conventional dendritic cells is required to survive a natural virus infection. *J. Virol.* **89**, 9974–9985 (2015).
30. A. Dahdah, K. Habir, K. S. Nandakumar, A. Saxena, B. Xu, R. Holmdahl, S. Malin, Germinal center B cells are essential for collagen-induced arthritis. *Arthritis Rheumatol.* **70**, 193–203 (2018).
31. J. A. Singh, D. E. Furst, A. Bharat, J. R. Curtis, A. F. Kavanaugh, J. M. Kremer, L. W. Moreland, J. O'Dell, K. L. Winthrop, T. Beukelman, S. L. Bridges Jr., W. W. Chatham, H. E. Paulus, M. Suarez-almazor, C. Bombardier, M. Dougados, D. Khanna, C. M. King, A. L. Leong, E. L. Matteson, J. T. Schousboe, E. Moynihan, K. S. Kolba, A. Jain, E. R. Volkmann, H. Agrawal, S. Bae, A. S. Mudano, N. M. Patkar, K. G. Saag, 2012 update of the 2008 American College of Rheumatology recommendations for the use of disease-modifying antirheumatic drugs and biologic agents in the treatment of rheumatoid arthritis. *Arthritis Care Res. (Hoboken)* **64**, 625–639 (2012).
32. Y. Ohtake, W. Kong, R. Hussain, M. Horiuchi, M. L. Tremblay, D. Ganea, S. Li, Protein tyrosine phosphatase σ regulates autoimmune encephalomyelitis development. *Brain Behav. Immun.* **65**, 111–124 (2017).

33. B. Bartok, D. L. Boyle, Y. Liu, P. Ren, S. T. Ball, W. D. Bugbee, C. Rommel, G. S. Firestein, PI3 kinase δ is a key regulator of synoviocyte function in rheumatoid arthritis. *Am. J. Pathol.* **180**, 1906–1916 (2012).
34. E. Beurel, S. F. Grieco, R. S. Jope, Glycogen synthase kinase-3 (GSK3): Regulation, actions, and diseases. *Pharmacol. Ther.* **148**, 114–131 (2015).
35. K. Singh, I. Colmegna, X. He, C. M. Weyand, J. J. Goronzy, Synoviocyte stimulation by the LFA-1-intercellular adhesion molecule-2-Ezrin-Akt pathway in rheumatoid arthritis. *J. Immunol.* **180**, 1971–1978 (2008).
36. T. Horbach, T. F. Chi, C. Götz, S. Sharma, A. H. Juffer, E. Y. Dimova, T. Kietzmann, GSK3β-dependent phosphorylation alters DNA binding, transactivity and half-life of the transcription factor USF2. *PLOS ONE* **9**, e107914 (2014).
37. S. K. Chang, Z. Gu, M. B. Brenner, Fibroblast-like synoviocytes in inflammatory arthritis pathology: The emerging role of cadherin-11. *Immunol. Rev.* **233**, 256–266 (2010).
38. Y. Wang, I. Shaked, S. M. Stanford, W. Zhou, J. M. Curtsinger, Z. Mikulski, Z. R. Shaheen, G. Cheng, K. Sawatzke, A. M. Campbell, J. L. Auger, H. Bilgic, F. M. Shoyama, D. O. Schmeling, H. H. Balfour Jr., K. Hasegawa, A. C. Chan, J. A. Corbett, B. A. Binstadt, M. F. Mescher, K. Ley, N. Bottini, E. J. Peterson, The autoimmunity-associated gene *PTPN22* potentiates toll-like receptor-driven, type 1 interferon-dependent immunity. *Immunity* **39**, 111–122 (2013).
39. G. S. Firestein, Rheumatoid arthritis in a mouse? *Nat. Clin. Pract. Rheumatol.* **5**, 1 (2009).
40. J. M. Alvaro-Gracia, N. J. Zvaifler, C. B. Brown, K. Kaushansky, G. S. Firestein, Cytokines in chronic inflammatory arthritis. VI. Analysis of the synovial cells involved in granulocyte-macrophage colony-stimulating factor production and gene expression in rheumatoid arthritis and its regulation by IL-1 and tumor necrosis factor-alpha. *J. Immunol.* **146**, 3365–3371 (1991).
41. F. C. Arnett, S. M. Edworthy, D. A. Bloch, D. J. Mcshane, J. F. Fries, N. S. Cooper, L. A. Healey, S. R. Kaplan, M. H. Liang, H. S. Luthra, T. A. Medsger, D. M. Mitchell, D. H. Neustadt, R. S. Pinals, J. G. Schaller, J. T. Sharp, R. L. Wilder, G. G. Hunder, The american rheumatism association 1987 revised criteria for the classification of rheumatoid arthritis. *Arthritis Rheum.* **31**, 315–324 (1988).
42. R. Altman, E. Asch, D. Bloch, G. Bole, D. Borenstein, K. Brandt, W. Christy, T. D. Cooke, R. Greenwald, M. Hochberg, D. Howell, D. Kaplan, W. Koopman, S. Longley III, H. Mankin, D. J. McShane, T. Medsger Jr., R. Meenan, W. Mikkelsen, R. Moskowitz, W. Murphy, B. Rothschild, M. Segal, L. Sokoloff, F. Wolfe, Development of criteria for the classification and reporting of osteoarthritis. Classification of osteoarthritis of the knee. Diagnostic and therapeutic criteria committee of the american rheumatism association. *Arthritis Rheum.* **29**, 1039–1049 (1986).
43. R. Altman, G. Alarcón, D. Appelrouth, D. Bloch, D. Borenstein, K. Brandt, C. Brown, T. D. Cooke, W. Daniel, D. Feldman, R. Greenwald, M. Hochberg, D. Howell, R. Ike, P. Kapila, D. Kaplan, W. Koopman, C. Marino, E. McDonald, D. J. McShane, T. Medsger, B. Michel, W. A. Murphy, T. Osial, R. Ramsey-Goldman, B. Rothschild, F. Wolfe, The american college of rheumatology criteria for the classification and reporting of osteoarthritis of the hip. *Arthritis Rheum.* **34**, 505–514 (1991).
44. C. Sacchetti, Y. Bai, S. M. Stanford, P. di Benedetto, P. Cipriani, E. Santelli, S. Piera-Velazquez, V. Chernitskiy, W. B. Kiosses, A. Ceponis, K. H. Kaestner, F. Boin, S. A. Jimenez, R. Giacomelli, Z.-Y. Zhang, N. Bottini, PTP4A1 promotes TGFβ signaling and fibrosis in systemic sclerosis. *Nat. Commun.* **8**, 1060 (2017).
45. M. Elchebly, J. Wagner, T. E. Kennedy, C. Lanctôt, E. Michaliszyn, A. Itié, J. Drouin, M. L. Tremblay, Neuroendocrine dysplasia in mice lacking protein tyrosine phosphatase σ. *Nat. Genet.* **21**, 330–333 (1999).
46. K. M. E. Andersson, M. N. D. Svensson, M. C. Erlandsson, I.-M. Jonsson, M. I. Bokarewa, Down-regulation of survivin alleviates experimental arthritis. *J. Leukoc. Biol.* **97**, 135–145 (2015).

Acknowledgments

Funding: This study was, in part, supported by funds from the NIH (R01 AR066053 and P30 AR073761), CDMRP (award W81XWH-16-1-0751), and MedImmune to N.B. This work was also supported by a Harrington Scholar-Innovator Award to N.B. from the Harrington Discovery Institute at University Hospitals in Cleveland, Ohio—part of The Harrington Project for Discovery & Development. M.N.D.S. was supported by a grant from the Arthritis National Research Foundation (632852). D.J.W. was supported by NIH Training Grant T32 AR064194. The work was also supported by grants from the Swedish Rheumatism Foundation (R-663971), the Sahlgrenska Academy and Sahlgrenska Hospital (ALFGBG-775731 and C4I-2018-01-10), and the Professor Nanna Svartz Foundation (2018-00251) to A.-K.H.E. In addition, this work was supported by a grant from the National Science Center in Poland (2016/23/B/NZ5/01469 to P.M. and grants from the Medical Research Council UK (PEAC grant 36661) and the Versus Arthritis Experimental Arthritis Treatment Centre (grant code 20022) to C.P. **Author contributions:** M.N.D.S., M.Z., S.Y., G.N., C.Se., K.M.D., K.S., F.M., F.H., R.H., E.S., C.Sa., K.W., D.J.W., C.B., R.A., W.W., P.M., T.K., D.L.B., and A.-K.H.E. contributed to acquisition and analysis of data. M.N.D.S., M.Z., S.Y., G.N., C.Se., K.M.D., F.G., D.V., M.L.T., S.R., M.B.B., G.S.F, C.P., A-K.H.E., S.M.S., and N.B. contributed to study conception and design. M.N.D.S., M.Z., S.Y., G.N., C.Se., K.M.D., D.J.W., C.B., K.L., F.M., R.A., W.W., G.P.S., F.G., M.L.T., S.R., M.B., G.S.F, C.P., A.-K.H.E., S.M.S., and N.B contributed to interpretation of data and manuscript preparation. **Competing interests:** The authors declare that they have no competing financial interests. **Data and materials availability:** Data used for the epigenomic analysis of RA and OA FLS are available in the Gene Expression Omnibus with the primary accession code GSE112658. Please address questions about the GSE112658 dataset to G.S.F. (gfirestein@health.ucsd.edu). RNA-seq data from freshly isolated RA FLS are available in the Gene Expression Omnibus with the primary accession code GSE109448. Please address questions about the GSE109448 dataset to M.B.B. (mbrenner@research.bwh.harvard.edu) or S.R. (soumya@broadinstitute.org). The PTPRS KO mice can be provided by M.L.T. pending scientific review and a completed material transfer agreement. Requests for the PTPRS KO mice should be submitted to michel.tremblay@mcgill.ca. Requests for the Fc-mTNFR should be submitted to ERA@amgen.com. All data needed to evaluate the conclusions in the paper are present in the paper and/or the Supplementary Materials. Additional data related to this paper may be requested from the authors.

Submitted 3 December 2019
Accepted 20 April 2020
Published 26 June 2020
10.1126/sciadv.aba4353

Citation: M. N. D. Svensson, M. Zoccheddu, S. Yang, G. Nygaard, C. Secchi, K. M. Doody, K. Slowikowski, F. Mizoguchi, F. Humby, R. Hands, E. Santelli, C. Sacchetti, K. Wakabayashi, D. J. Wu, C. Barback, R. Ai, W. Wang, G. P. Sims, P. Mydel, T. Kasama, D. L. Boyle, F. Galimi, D. Vera, M. L. Tremblay, S. Raychaudhuri, M. B. Brenner, G. S. Firestein, C. Pitzalis, A.-K. H. Ekwall, S. M. Stanford, N. Bottini, Synoviocyte-targeted therapy synergizes with TNF inhibition in arthritis reversal. *Sci. Adv.* **6**, eaba4353 (2020).

Synoviocyte-targeted therapy synergizes with TNF inhibition in arthritis reversal

Mattias N. D. Svensson, Martina Zoccheddu, Shen Yang, Gyrid Nygaard, Christian Secchi, Karen M. Doody, Kamil Slowikowski, Fumitaka Mizoguchi, Frances Humby, Rebecca Hands, Eugenio Santelli, Cristiano Sacchetti, Kuninobu Wakabayashi, Dennis J. Wu, Christopher Barback, Rizi Ai, Wei Wang, Gary P. Sims, Piotr Mydel, Tsuyoshi Kasama, David L. Boyle, Francesco Galimi, David Vera, Michel L. Tremblay, Soumya Raychaudhuri, Michael B. Brenner, Gary S. Firestein, Costantino Pitzalis, Anna-Karin H. Ekwall, Stephanie M. Stanford and Nunzio Bottini

Sci Adv **6** (26), eaba4353.
DOI: 10.1126/sciadv.aba4353